

STUDY OF SPIN DEPENDENT TUNNELING IN DOUBLE
BARRIER MAGNETIC TUNNEL JUNCTIONS



MS Research Thesis

By

Fahad Hassan

278-FBAS/MSPHY/S14

Supervisor

Dr. Naeem Ahmad

DEPARTMENT OF PHYSICS
FACULTY OF BASIC AND APPLIED SCIENCES
INTERNATIONAL ISLAMIC UNIVERSITY, ISLAMABAD



★
Accession No. TH1258 ^{MS}

MS
621.381

FAS

Fabrication of CoFeB.
X-Ray diffraction.
UV Lithography.

Acknowledgements

I would like to quote that this work would not have been possible without the support of some people who were always there to help and support me. The very first I would like to thank my supervisor, Professor **Dr. Naeem Ahmad**, for his help, support, generosity and the worthy ideas for the success of this work. I would also like to thank the HOD of the department of physics, IIUI, **Dr. Waqar Adil Syed** and other faculty members for their valuable discussions and suggestions on my research work. I also thank Mr Ahmad Shryar and Mr. Muhammad Ali from advanced electronics lab, IIUI, for his support in different characterizations. I would also like to thank Dr. Volker Neu from Institute for Matellic Materials Germany for his support in characterizations of samples. I would like to thank my friends and colleagues at Spintronic lab, IIUI, for their help and inspiration. I thank Mr. Ahmad Saeed, Mr. Usama Bashir, Mr. Muhammad Salman and Mr. Affan safeer for their valuable advices and huge support on my research. Furthermore, I would like to thank my family and friends for their immeasurable support. Thank all of you; this MS would not have been possible without you.

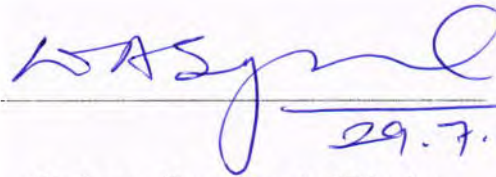
STUDY OF SPIN DEPENDENT TUNNELING IN DOUBLE BARRIER MAGNETIC TUNNEL JUNCTIONS

BY:

Fahad Hassan

(278-FBAS/MSPHY/S14)

This thesis is submitted to department of physics International Islamic University Islamabad,
for the award of degree of MS Physics



Chairman Department of Physics

**CHAIRMAN
DEPT. OF PHYSICS
International Islamic University
Islamabad**

29.7.16

International Islamic University Islamabad.



Dean Faculty of Basic and Applied Sciences

International Islamic University Islamabad.

International Islamic University, Islamabad

Faculty of Basic and Applied Sciences

Department of Physics

Final Approval

It is certified that the work presented in this thesis entitled "STUDY of SPIN DEPENDENT TUNNELING IN DOUBLE BARRIER MAGNETIC TUNNEL JUNCTIONS"

By **Fahad Hassan**

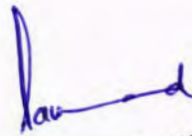
Registration No.278-FBAS/MSPHY/S14

is of sufficient standard in scope and quality for the award of degree of MS (Physics) from International Islamic University, Islamabad.

Committee

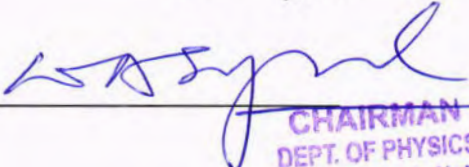
External Examiner

Dr. Javed Iqbal Saggu
Assistant Professor,
Department of Physics,
Quaid-i-Azam University, Islamabad


DR. JAVED IQBAL SAGGU
Assistant Professor
Department of Physics
Quaid-e-Azam University
Islamabad

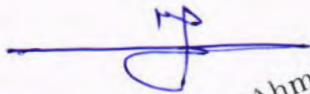
Internal Examiner

Dr. Waqar Adil Syed
Associate Professor,
Chairman, Department of Physics
International Islamic University, Islamabad


CHAIRMAN
DEPT. OF PHYSICS
International Islamic University
Islamabad

Supervisor

Dr. Naeem Ahmad
Assistant Professor,
Department of Physics
International Islamic University, Islamabad


Dr. Naeem Ahmad
Assistant Professor (Physics)
International Islamic University
Islamabad

Dated: 01-07-2016

Declaration

I hereby declare that this thesis work, neither as a whole nor a part of it has been copied out from any source. Further, work presented in this dissertation has not been submitted in support of any application for any other degree or qualification to any other university or institute. If any part of this project is proved to be copied from any source or found to be reproduction of some other project, I shall be legally responsible for punishment under the plagiarism rules of Higher Education Commission (HEC), Pakistan.

Fahad Hassan

(278-FBAS/MSPHY/S14)



**INTERNATIONAL ISLAMIC UNIVERSITY,
ISLAMABAD
Faculty of Basic and Applied Sciences
Department of Physics**

MS THESIS COMPLETION CERTIFICATE

Mr. **Fahad Hassan** Registration No. **278-FBAS/MSPHY/S14** student of Master of Science has submitted his research thesis titled “STUDY of SPIN DEPENDENT TUNNELING IN DOUBLE BARRIER MAGNETIC TUNNEL JUNCTIONS”.

His thesis is complete in all aspects and ready for external examination. The plagiarism report is also enclosed here with, which is in acceptable range.

(Dr. Waqar Adil Syed)
Chairman, department of
Physics, IIU Islamabad

بِسْمِ اللَّهِ الرَّحْمَنِ الرَّحِيمِ

DEDICATED
To
MY BELOVED PARENTS

Contents

Abstract.....	3
Motivation.....	4
Thesis outline.....	5
CHAPTER 1 Introduction to Nano Technology.....	6
1.1 Introduction.....	6
1.2 Background.....	7
1.3 Recent developments.....	8
1.4 Introduction to magnetism.....	9
1.5 Magnetic tunnel junctions.....	12
1.6 Theory of magnetic tunneling.....	13
1.6.1 Julliere model.....	13
1.7 Tunneling effect.....	15
1.8 Magnetoresistance.....	17
1.8.1 Giant Magnetoresistance.....	17
1.8.2 The TMR effect.....	21
1.9 Spin-Transfer Torque (STT) Domain Wall Motion.....	23
1.10 Spin Hall Effect.....	25
CHAPTER 2 Synthesis and Fabrication.....	28
2.1 Synthesis of Nanomaterials.....	28
2.2 Top-down and Bottom-up approach:.....	28
2.3 Sputtering:.....	28
2.3.1 DC diode sputtering:.....	28
2.3.2 RF diode sputtering:.....	29
2.3.3 Magnetron sputtering:.....	30
2.4 UV Lithography:.....	31
2.5 Ion-beam etching:.....	32
2.6 Electro deposition Technique.....	33
2.6.1 Template assisted electrochemical deposition.....	34
2.6.2 Types of Electrodeposition.....	34
2.7 CoFeB /Al-O/ CoFeB/Al-O/CoFeB Double barrier magnetic tunnel junctions:.....	35
2.8 Fabrication of Magnetic Tunnel Junction:.....	37

2.8.1 Step 1: Fabrication of bottom electrode.....	37
2.8.2 Step 2: Fabrication of tunnel junction:.....	38
2.8.3 Step 3: Fabrication of Top Electrode:.....	39
2.9 Fabrication of CoFeB thin film.....	40
CHAPTER 3 Experimental Techniques.....	42
3.1. X-Ray Diffraction (XRD):.....	42
3.1.1 Production of X-rays:.....	42
3.1.2. Bragg's Law:.....	43
3.2. Scanning Electron Microscopy:.....	44
3.3 Two Point Probe Method:.....	46
3.3.1 Problems of two probe method:.....	46
3.4. Four point probe method:.....	47
3.4.1 Measuring resistance of MTJ by Four point Probe method:.....	47
3.5 Vibrating Sample Magnetometer (VSM).....	48
CHAPTER 4 Results and conclusion.....	50
4.1 Transport Properties of CoFeB/Al-O/CoFeB:.....	50
4.2 TMR for the MTJ with glass substrate:.....	50
4.3 Effect of change of substrate in CoFeB/Al-O/CoFeB MTJ:.....	51
4.4 I-V Characteristic Curve for DBMTJ with glass substrate:.....	53
4.5 I-V Characteristic Curve for DBMTJ with SiO ₂ substrate:.....	55
4.6 Hall measurements for DBMTJ:.....	55
4.7 SEM images of CoFeB thin film.....	57
4.8 EDS results of CoFeB thin film.....	58
4.9 I-V characteristics of CoFeB thin film.....	59
4.10 Hall measurements for DBMTJ and CoFeB thin film:.....	60
4.10.1 Hall measurements for CoFeB thin film:.....	60
4.11 M-H loops of CoFeB thin films.....	65
Conclusion.....	67
References.....	68

Abstract

Magnetic tunnel junctions (MTJs), are made by sandwiching a very thin insulating layer between two ferromagnetic (FM) layers. If the tunnel barrier is replaced by two tunneling barriers around an intermediate layer of ferromagnetic material it is called a double barrier magnetic tunnel junction, this type of magnetic tunneling junction could gain new properties. Magnetic tunnel junctions could be called the key devices in the emerging spintronic technology and they have a vast application in computer devices such as hard disk drives, Magnetic random access memory (MRAM) and future spintronic devices. The work presented here is related to the fabrication and characterization of double barrier magnetic tunnel junction and to observe the phenomenon of tunneling magnetoresistance (TMR) and the effect of different substrates on the TMR values. We have also worked on the development of spin hall effect in the junction and found that it could have effect in the switching of the magnetization direction of FM layers. The fabrication of CoFeB/Al₂O₃/ CoFeB/Al₂O₃/CoFeB was undertaken using the magnetron sputtering system at base pressure $P=10^{-8}$ Torr, photolithography and ion beam etching. Tunneling Magnetoresistance (TMR) of up to 37% was obtained from MTJs with a layer structure of Ru/Cu/Ru/IrMn/CoFe/Ru/CoFeB/Al₂O₃/ CoFeB/Al₂O₃/CoFeB/Ta/Ru/SiO₂. We have used two different substrates 1) glass 2) SiO₂. It is found that the change of substrate results in the change of TMR. We have also studied the magnetic properties of CoFeB thin films. The film deposition, for the evaluation of spin Hall Effect and magnetic measurements was done and characterized for required measurements. The values of resistivity for CoFeB thin film shows that for sample prepared for 5 min deposition time have max resistivity which decreases for higher deposition time and has gradual increase at the end but still not comparable to the sample 1. Which shows that the optimized conditions to gain max resistivity are as for sample 1. We conclude that for a specific thickness of film the resistivity is maximum. The value of resistance for CoFeB thin films fluctuate between 3 to 17 Ω . The magnetic measurements, TMR, spin Hall Effect, carrier concentration, charge mobility, effect of different variation in sample preparation have been systematically studied to achieve desired magnetic properties of layer stacks.

Motivation

Magnetic tunnel junctions (MTJ) are one of the main devices in the field of spintronics with the application in emerging technology of computer hard disc drives, magnetic random access memory (MRAM) and other spintronic devices. There is always a constant need to increase the storage density in hard disk drives and MRAM technology and to acquire new MTJ materials and structures to increase the tunneling magneto resistance (TMR) and more vigorous process conditions for integration of MTJs. This emerging development inspires the need for the research to improve the understanding of the science and relevant physical phenomena collaborated with these devices. The purpose of this work is to provide new approach for the development of MTJ devices for the applications in different devices. The challenges related includes the development of basic film deposition for MTJs with CoFeB as FM layer and AlO barriers and to study the TMR phenomenon at room temperature and at low temperature as well. Magnetic properties, Spin transfer torque and spin Hall Effect is also studied.

Thesis outline

The thesis is organized as follows.

Chapter 1 is the motivation and introduction about the magnetic tunnel junction and spin hall effect. A brief description on the history, background knowledge and recent development in relevant topics about MTJs is given.

Chapter 2 gives the synthesis techniques and experimental methods adapted for the fabrication of MTJ and CoFeB thin film which includes thin film deposition techniques, magnetron sputtering, photolithography and electro deposition.

Chapter 3 present the detail about the characterization techniques employed for obtaining the desired results these characterizations includes TMR measurements, I-V curve measurements, SEM, XRD, Hall measurements.

Chapters 4 present detailed results obtained in this work including tunneling magnetoresistance, I-V curves, Spin Hall Effect occurrence and its effect on the magnetization switching.

CHAPTER 1 Introduction to Nano Technology

1.1 Introduction

Over the last six decades electronics technology has been overcome by the idea of developing charge sophisticated devices for a number of applications which includes digital memory, digital logic and amplification of analog signal manipulation have emerged on the bases of this concept. The physics of charge transport in different metals and semiconductors has lead the way for the triumph of twentieth century solid state physics and material science. However, in the past decade, we have seen a rapid development of a new phenomenon which employs not only the charge of electron but also the spin of electron that lay the foundation of spintronics. AlO_x is a commonly used material for barrier making in MTJs to obtain high TMR at room temperature. AlO_x is formed by the oxidizing the pre deposited Al layer. The MTJ with a sandwich structure if FM/I/FM and spin dependent transport properties have drawn a wide interest resulting in the large magnetoresistance MR ratio of 81% at room temperature and 107% at 4.2 K using an AIO barrier. There are different types of AIO barrier based MTJs that include spin valve type pinned MTJ, double barrier magnetic tunnel junctions DBMTJ, perpendicular anisotropic MTJ, Half metal MTJ, dilute magnetic semiconductor composite MTJ, superconductor composite MTJ, granulate film composite MTJ and nano ring shaped MTJ etc. Immense research is done in this field for the practical application in the devices. The field of spintronics has emerged rapidly by the discovery of spin transfer torque SST effect, it was a remarkable achievement in the development process. This effect is consistent with development of high density devices and it also provides new strategy for data writing. The pursuing target is to reduce the critical switching current both in lab and industry as well. Magnetic read head, magnetic sensors, MRAM, spin and field effect transistors are some important applications of AIO based MTJs.

The advancement in the spin based electronic or spintronics paves new ways of manipulating charge which was previously not possible in charge base electronics, also offering potential advantages in speed, density, power and reliability [1]. The spintronic devices are mainly incorporate magnetic materials in the path of conduction of electrons. For example ferromagnetic materials often incorporated to produce a spin polarized current in which the spin orientation of one type is greater than the other among the conduction electron. The spin imbalance can be

summarized in a number of ways. John Slonczewski and Luc Berger, two theorists predicted that passing the spin polarized current through ferromagnets results in the absorption of transverse component of spin from electron by the local moment of FM [2 3]. When conduction electron transfers an angular momentum to ferromagnet it result in a torque on that ferromagnet and this torque can be used directly for the switching of magnetization in FM. This effect is verified in both point contacts experimentally [4 5].

A spin valve is a typical structure which includes a large F layer known as fixed layer used to polarize the electron spin in current. A second small layer which is called free layer, responds to torque. A large current density of order 10^7 - 10^8 A/cm² is applied to observe the effect in transition metals because the total spin transfer per electron is relatively small. The generation of Oersted field by the current itself can be an influence on the magnetization of free layer unless the current is confined to nanoscale dimension (200nm) [6]. The field of spin transfer is growing rapidly. This effect has been studied in the different devices. In 2004, Grandis Corporation and one other group at Cornell have demonstrated spin transfer switching in MTJs with a very thin AlO_x tunnel barrier [7 8]. Within the time of a few months, further spin transfer torque have been used to push domain walls in the ferromagnetic wires of nano scale. [9 10] and also the switch of magnetization in semiconductors magnetic devices at low temperature [11 12]. There are very promising potential applications in addition to the nanoscale physics. For example, we can use spin transfer torque to write low power, high speed and nonvolatile dense magnetic memory on the MTJ bits. MRAM, the application of magnetic memory are used for switching the MTJs magnetic write scheme is used for this purpose and the device has been developed by some companies in U.S [13 14]. Since the cell size is scaled down the power required for the field writing scales up. Therefore, the power requirements scale up with the cell area so spin transfer writing is considered as the alternative.

1.2 Background

The central concept of spintronics is to use the spin degree of freedom of electron to develop devices which are faster with multifunctional properties and which consume less energy as well. In the past few years there have been huge developments in the field of spintronics that made a breakthrough in the conventional electronic technology. Due to its basic research and industrial application MTJ has become most important devices of spintronics, such as MRAMs, hard disc

drive and magnetic sensors. Basic concepts of MTJ and spin hall effect in ferromagnets are introduced in this thesis.

Recent developments

Nowadays magnetic tunneling junctions are used widely for the structures based on the principle of spintronics. Using the phenomenon of spintronics in different devices we can take the advantage of both the charge of electron as well as its spin. This phenomenon is used in different devices like field sensors, magnetic memories or logic devices, Magnetic random access memory MRAM etc. Magnetic tunneling junctions are composed of two layers of ferromagnetic material separated by very thin layer of insulator. Tunneling effect occurs for the transport of electrons through these junctions. The electrical resistance depends on the relative orientation of the ferromagnetic material layer which makes it very interesting for different applications. The resistance is low when the magnetization are parallel and high when the magnetizations are antiparallel.

If the tunnel barrier is replaced by two tunneling barriers around an intermediate layer the magnetic tunneling junction could gain new properties. Double barrier junctions could pave the way towards new devices such as spin diode [15] or spin transistor [16]. Therefore a clear understanding of spin dependent transport properties in these double barrier junctions is necessary. In fact these structures behave differently from single barrier junction. It is observed that double junctions may present a specific signature when current flows in the plane of the layers [17]. Moreover an amplification of spin transfer torque in these double junctions is also observed. It is demonstrated that the hysteresis-free MR loop can be obtained in a free layer thickness range by controlling the annealing temperature [18].

The spin conservation in electron tunneling gives rise to the possibility of spin sensitive tunneling between two ferromagnets (FM) layers which leads to a large magneto resistance (MR) values > 30% at room temperature. This recent success has led to several fundamental questions regarding the phenomenon of spin tunneling, besides showing tremendous potential for applications as nonvolatile magnetic memory elements, read head and picotesla sensors [19 20]. Thermally assisted MRAM devices with sizes and electrical properties relevant for nonvolatile memory can be made to survive the high process temperatures required for embedded CMOS memory and also have low read and write fields. Devices were shown to survive 10^8 write cycles. This may open up new applications of MRAM [21].

Control of the crystallization of the middle CoFeB layer is important for optimizing the MTJ with double MgO barriers, and especially for the fabrication of double barrier MTJ on a large area substrate [22].

Experimental work is reviewed with the emphasis on projected applications, in which external electric and magnetic fields will be used to control spin and charge dynamics to create new functionalities not feasible or ineffective with conventional electronics.

Spintronics is being used in lot of applications like ferromagnet/insulator/superconductor (F/I/S) tunneling, F/I/F tunneling, Andreev reflection, Spin-polarized drift and diffusion, Materials considerations, Spin filters, Spin diodes, Spin transistors, Spin field-effect transistors, Magnetic bipolar transistor, Hot-electron spin transistors and Spin qubits in semiconductor nanostructures. We shall discuss the experimental results and the current theoretical understanding of spin dependent tunneling in Spintronics nanostructures: its dependence on bias, temperature and barrier characteristics [23 24].

1.4 Introduction to magnetism

Magnetism exists in almost all the materials and is due to the tiny magnetic moments and their orientation. These moments are the result of orbital and spin magnetic moments together. Orbital magnetic moment is the result of motion of the electrons around the nucleus constituting current and gives perpendicular to the orbit plane magnetic moment. Spin magnetic moment is due to intrinsic angular momentum of electrons. Magnetization M of the material describes the strength of the magnetism of that material. Which can be defined as the magnetic moment per unit volume of the particular substance. When the material is placed in some external magnetic field H , there is a relationship between M and H as

$$\vec{M} = \chi \vec{H} \quad (1)$$

Where χ is called the magnetic susceptibility. Different material can be categorized as diamagnetic, paramagnetic, ferromagnetic and anti-ferromagnetic materials depending on the sign and order of the magnitude of χ . For diamagnetic materials we have negative χ and of the order 10^{-5} that is due to contribution of orbital magnetic moments. Diamagnetism exist in almost all the materials but it is so weak that it is overcome by Para magnetism or in most cases ferromagnetism.

Magnetization is proportional to the external field and the susceptibility is of the order 10^{-3} to 10^{-5} , for Para magnetism. It is because of the spin moments of unpaired electrons in the atom or ion. These spin moments produce a very weak magnetization when they are in a magnetic field and are isolated from each other. By the removal of external field the magnetization will be zero due to the thermal agitation. Even if the order of magnitude of susceptibility is very small in diamagnets and para magnets, the effect on overall magnetic signal with very thin FM layer containing sample may not be negligible. It is therefore very important to choose the right materials for sample holder or rod for building highly sensitive magnetometers, for example vibrating sample magnetometer (VSM). We are mainly focused on ferromagnetism and anti-ferromagnetism for MTJs. Since no external field is required to introduce the magnetization, the magnetic ordering is spontaneous in ferromagnets and anti-ferromagnets. Weiss's molecular field theory and Heisenberg's quantum mechanical exchange interaction theory [25 26], in magnetic materials spontaneous magnetization originates by the exchange interactions in spin moments of unpaired electrons of neighbor atoms. This internally produces quantum mechanical force by which the moments of individual atom is aligned in parallel or anti-parallel state which is known as magnetic ordering.

Fig 1.1 shows two forms of magnetic order which is (a) FM ordering (b) AFM ordering

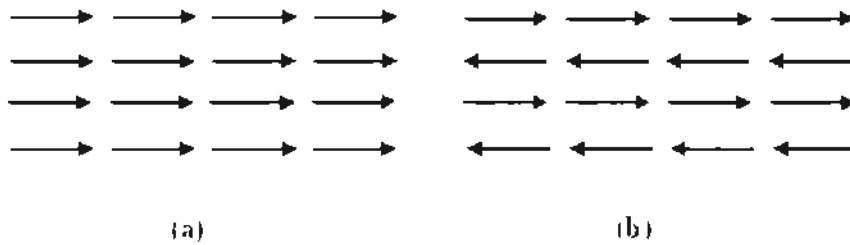


Fig. 1.1: Schematic illustrations of magnetic ordering. (a) The magnetic moments are aligned parallel in a FM material due to the strong positive exchange interactions between the spin moments. (b) The magnetic moments are aligned anti-parallel in an AFM material due to the strong negative exchange interactions between the spin moments.

Due to the strong +ve exchange interactions or we can call FM coupling, the spin moments of adjacent atoms align parallel in FM ordering, as shown in the Fig. 1.1 (a). These regions are described as magnetic domains. Even if the magnetic moments in FM materials are aligned naturally within the domain, there is a possibility that because of the random orientation of domain magnetization in the absence of magnetic field no magnetization is exhibited by FM materials. Saturation magnetization of spontaneous magnetization M_s

is the magnitude of single domain magnetization. Due to thermal effects the saturation magnetization vanishes above a critical temperature, which is called Curie temperature (T_C). In an antiferromagnetic coupling is negative between the adjacent atomic moments and spin moments are antiparallel in neighboring layers as shown in Fig.1.1 (b). Which result in zero net magnetization. Above a certain temperature material becomes paramagnetic and AFM ordering becomes random, this temperature is known as the Neel temperature (T_N).

When the spin moments in neighboring atoms are antiparallel due to negative exchange interaction while the net magnetization is due to the unequal atomic moments of neighboring atoms the material is called a ferrimagnet.

By the MH or hysteresis loop as shown in the Fig.1.2. we can understand the behavior of a ferromagnetic material placed in an external applied field H. the magnetization of the material that is never been magnetized or demagnetized will follow the dashed line when we start from $H=0$ and will reach the saturation point of magnetization M_s as the H increases. The magnetization is aligned to the field direction for all the domains (a in Fig.1.2)

Magnetization remains non zero even if the applied field is decreased. Remanent magnetization M_r is the value of net magnetization at this point. Here some domains remain aligned and some lose their alignment. By reversing the magnetic field to point b the magnetization is reduced to zero. This magnetic field required to reduce the magnetization to zero is called coercivity H_c . By reversing the field to point b the magnetization reaches to zero. The magnetic field value required for the reduction of magnetization to zero is called coercivity. By the increase in the strength of field in opposite direction, again, the domains become aligned and at point c they saturate in opposite direction. Again reversing the field results in magnetization reduction

Where P_1 is spin polarization for FM1 and P_2 is the spin polarization for FM2. P is calculated from the spin dependent density of state at E_F .

$$P_i = \frac{N_{i\downarrow}(E_F) - N_{i\uparrow}(E_F)}{N_{i\uparrow}(E_F) + N_{i\downarrow}(E_F)}, i = 1, 2$$

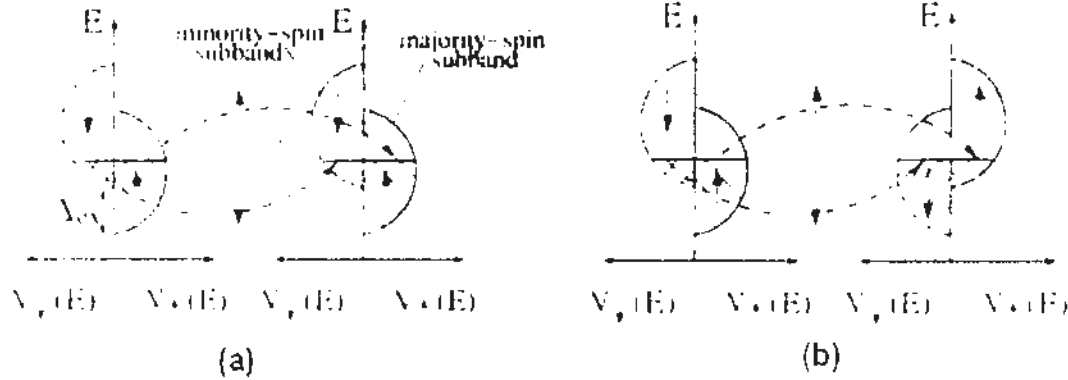


Fig. 1.3: Schematic illustration of spin dependent tunneling in an MTJ: (a) parallel and (b) antiparallel alignment of the two FM electrons.

From equation (27) we can see that TMR is polarization dependent of FM layer. The spin polarization is an intrinsic property of the ferromagnetic material. When we have nonmagnetic material $P = 0$ and when we have half metal material that is spin polarized fully then $|P| = 1$. Equation (11) depicts that by higher polarization materials we can get higher TMR. If we use half metals there will be indefinite TMR. A very high TMR is reported in MTJs using half metals at low a temperature [28 29]. However, at room temperature high TMR has never been observed yet for half metal electrodes.

Julliere's can be said as an approximate description of TMR effect. The 70% TMR of the MTJs having 3d FM alloy electrodes is close to the Julliere limit which is estimated from the experimental values of the spin polarization. However, the model is unable to explain the ultra-high value of TMR in MTJs having MgO barriers. This could be due that Julliere model does not consider the effect of the tunnel barrier on the TMR.

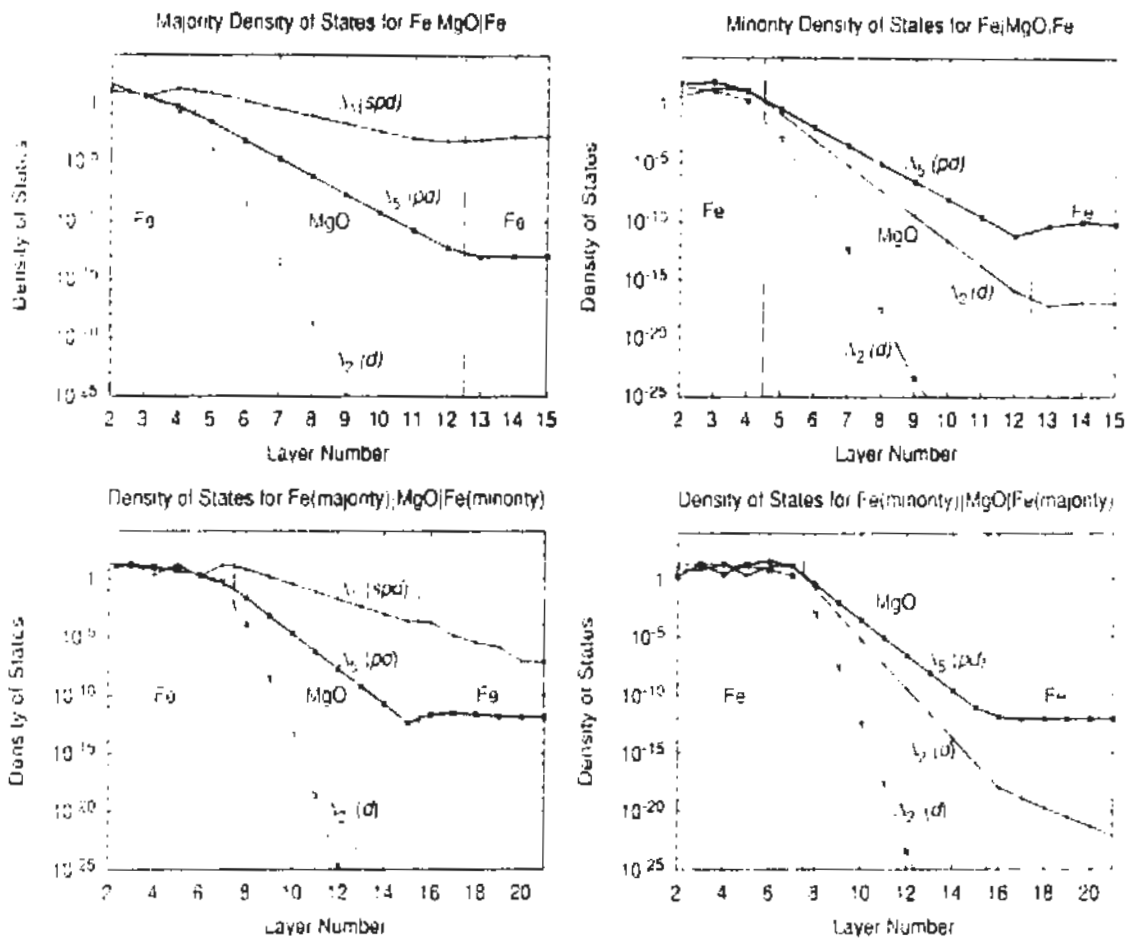


Fig. 1.4: Tunneling DOS for Fe(100)/MgO/Fe(100) for parallel alignment of magnetizations majority (a), minority (b), and antiparallel alignment of magnetizations (c) and (d)[30].

1.7 Tunneling effect

It is a quantum mechanical effect which means that an electron can transmit through a higher kinetic energy barrier as compared to the energy of electron itself. Classical physics cannot explain this phenomenon. According to quantum mechanics we consider that due to wave properties of electron it is possible that the wave can transmit through barrier. Here, tunneling effect is demonstrated by a possible current flow through a very thin insulating layer between two FM metals. Fig 1.5 shows a barrier that is rectangular and describes metal/insulator/metal condition. Electrons having energy $E < V_0$ travel in x in rectangular barrier. To simplify the problem it is considered that are identical having perfect interface.

$$V(x) = \begin{cases} V_0, & 0 \leq x \leq a \\ 0, & x < 0, x > a \end{cases} \quad (5)$$

Where V_0 is the energy height of the barrier.

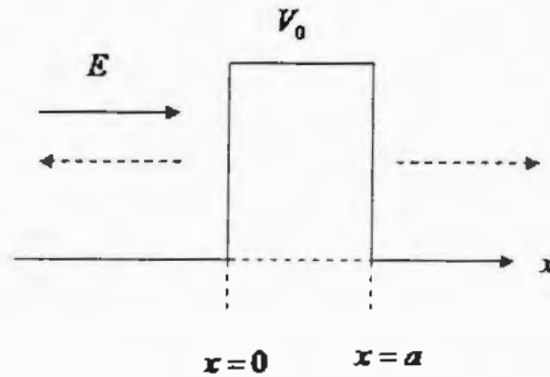


Fig. 1.5: Rectangular tunneling barrier.

By solving the time independent one dimensional Schrödinger equation:

$$E\psi(x) = \left[-\frac{\hbar^2}{2m} \nabla^2 + V_0 \right] \psi(x) \quad (6)$$

Where $\hbar = h/2\pi$, h is Planck's constant and m is the mass of the particle. The

solutions are:

$$\psi(x) = \begin{cases} Ae^{ik_1x} + Be^{-ik_1x}, & (x \leq 0) \\ Ce^{ik_2x} + De^{-ik_2x}, & (0 \leq x \leq a) \\ Fe^{ik_1x}, & (x \geq a) \end{cases} \quad (7)$$

Where k_1 and k_2 are the wave numbers with $k_1 = \sqrt{2mE/\hbar^2}$ and $k_2 = \sqrt{2m(V_0 - E)/\hbar^2}$. In the area of $x \leq 0$, both incident wave Ae^{ik_1x} and

Reflected wave Be^{-ik_1x} exist, while in the area of $x \geq a$, only the transmitted wave

$F e^{ik_2x}$ Exists. Due to the conditions that exist at the boundaries of the barrier, both the wave functions and their differentials must be continuous, the constants B, C, D and F are found to be correlated to A . The ratio of the transmitted current density $|F|^2$ to the incident current density $|A|^2$ is defined as the transmission coefficient:

$$T = \frac{|F|^2}{|A|^2} = \frac{4k_1^2 k_2^2}{(k_1 + k_2)^2 \sin^2 k_2 a + 4k_1 k_2} \quad (8)$$

$$\approx \frac{16E(V_0 - E)}{V_0^2} e^{-\frac{2a}{\hbar} \sqrt{2m(V_0 - E)}}$$

It can be seen that the incident electron can be transmitted despite the barrier height exceeding its energy, and the transmission T is dependent on the barrier width a .

$(V_0 - E)$, incident particle mass m , decreasing exponentially as a increases.

1.8 Magnetoresistance

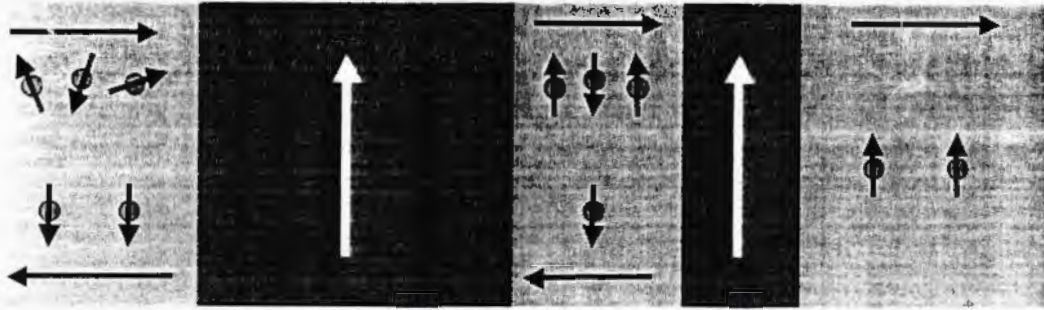
The change in the resistance of some conductor with the applied magnetic field is called magnetoresistance MR. large MR effects up to several 100 % are observed in magnetic materials due to spin polarization of electrons. The GMR and TMR effects are explained below.

1.8.1 Giant Magnetoresistance

The conduction electrons are un-polarized in a normal conductor wire. If we insert a ferromagnetic material into the wire we impose a direction quantization on the electrons in the wire through the exchange interaction the ferromagnetic material. The quantization direction is the direction of

local magnetization in ferromagnet. Spin polarized current is generated in F bulk and F/N interface through spin dependent scattering. In terms of two parallel resistance channels the system can be modeled where the orientation of each spin feels different resistance for F/N and F layer [31]. An F/N/F multilayer stack is shown in fig. 1.5 where the resistance is depending upon the relative angle between the F layers. The devices are patterned with an elongated shape often as shown in fig 1.6 c, it is to align the equilibrium position of F layer either parallel or antiparallel w.r.t each other. The resistance is low if the F layers are parallel aligned for typical F & N layers since the two spin channels are scattered by the two F layers. If the F layers are aligned antiparallel, in both channels a strong scattering occurs which causes a large resistance fig 1.5. This effect allows us to interpret the measurements of resistance in terms of relative angle of magnetization and is known as giant magnetoresistance GMR [32]. The two F layers are made of different thickness to break the symmetry between the layers. The layer which is thicker is referred as fixed layer while the layer which is thin is referred as free layer. A typical measurement of the GMR response is shown in Figure 1.6(b). As the magnetic field is cycled about the free layer magnetic hysteresis loop, the differential resistance (dV/dI) is measured before starting the measurements the orientation of fixed layer is set to positive magnetic field direction. Within the range of applied field this layer does not switch in this measurement. The Nano magnets which make the fixed and free layer, exert magneto static field called dipolar field (H_{dip}) on each other. From the field offset in GMR loop of free layer, magnitude of fixed and free layer (H_{dip}) can be measured fig 1.6 b.

Parallel alignment - Low resistance



Anti-parallel alignment - High resistance

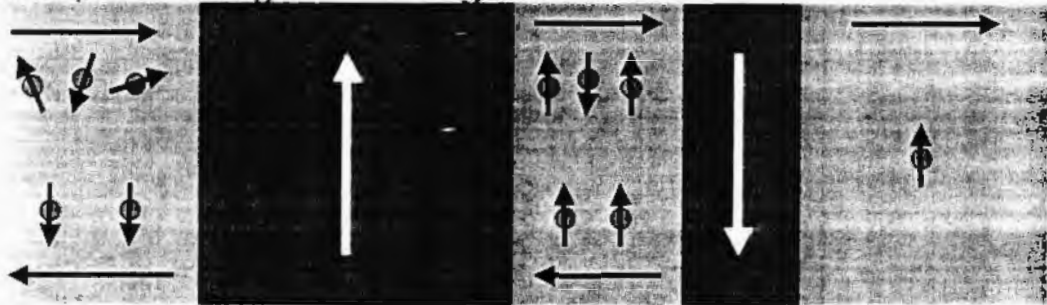


Figure 1.5: Simplified cartoon model of interfacial spin-dependent scattering in a standard spin valve structure. At the first N/F interface, un-polarized spins from the leads are preferentially aligned or anti-aligned with the magnetization. The spins that are aligned with the magnetization are preferentially transmitted (they see a small interfacial resistance), and the ones anti-aligned are preferentially reflected (they see a larger interfacial resistance). When the two moments are aligned parallel (top), there is no strong spin scattering for the spin up electrons, which results in a net larger conductance (lower resistance). When the moments are aligned antiparallel (bottom) then strong scattering occurs for both spin up and down electrons, which causes a net smaller conductance (larger resistance).

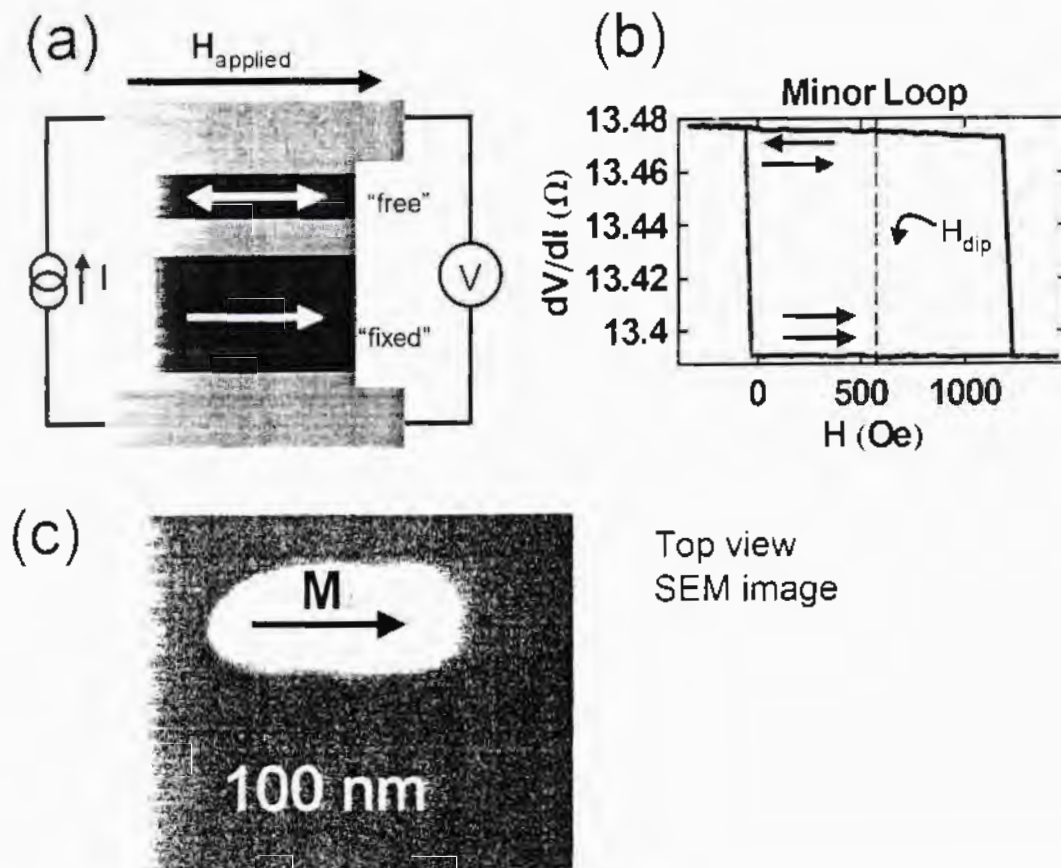


Figure 1.6: (a) Basis dc measurement scheme for current perpendicular-to-the plane (CPP) GMR. (b) Plot of differential resistance (dV/dI) vs. H_{applied} that describes the hysteresis of the free layer, while the fixed layer is aligned with the $+H_{\text{applied}}$ direction. The shift of the loop from $H_{\text{applied}} = 0$ is equal to the dipolar field, H_{dip} , of the fixed layer. (c) Top view SEM image of a e-beam fabricated ion mill mask with dimensions similar to the spin valve measured in (b). Nominal dimensions are 55x127 nm.

1.8.2 The TMR effect

The MTJ consist of a very thin layer of insulator sandwiched by two FM layers. It is designed in such a way that the field for switching is different for each layer. Which concludes that each FM layer have different H_c . The layer with lower H_c is called soft layer or free layer and the other with the higher H_c is hard or pinned layer. There are a number of methods for producing H_c for the FM layers. For example to choose the FM materials having different H_c . The other is to use different shape anisotropy for the same FM layers but having difference in thickness or shape. The magnetization of one of FM layer is fixed or pinned by the exchange bias of an adjacent AFM layer is one of the most effective way to get switching at low field (as considered in practical application). The layer which is unpinned is called free layer while the pinned layer is exchange bias layer. As shown in the Fig.1.7. the dependence for the magnetization alignment of pinned and free layers on the applied field is shown in fig 1.8 (a) in which the hysteresis loops that are one which is around the zero field is from free layer contribution and other around H_{ex} is from the contribution of pinned layer due to the bias effect. H_{ex} is the exchange bias field that is produced in AFM or FM bilayer system. In fig 1.8 (b) is shown the dependence of resistance of MTJ on the magnetic field alignment of relative to the pinned and free layer. The MTJ is at low state when the magnetization of two FM layers are parallel and at high state when the magnetizations are anti parallel. TMR is defined as

$$TMR = \frac{R_{AP} - R_P}{R_P} \quad (9)$$

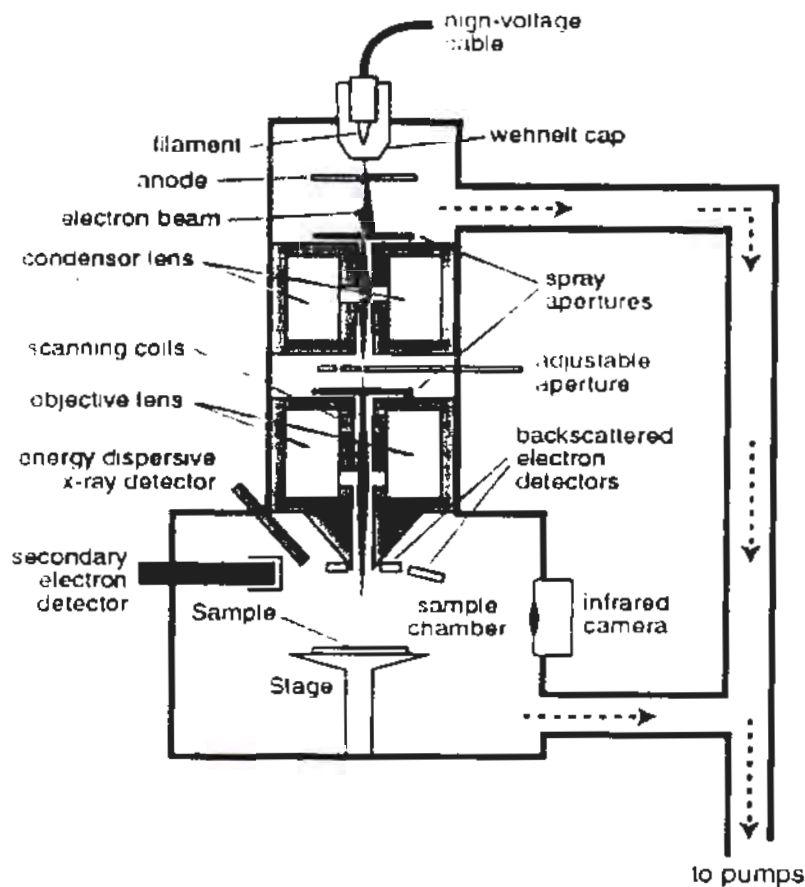


Fig. 3.4: Schematic diagram of Scanning electron microscope

Different parts used in SEM are heating filaments conducting lenses, objective lenses, electron gun and aperture. Electron gun emits the electrons which are accelerated through gaining KE by applying high voltage of 100eV to 100 KeV between anode and filament. Verity of pulses of signals are produced by the emitted electrons when they gain KE.

Backscattered electrons, diffracted electrons, secondary electrons, heat, visible light and photons are parts of these pulses of signals. For sample imaging back scattered and secondary electrons are used. For topography and surface morphology secondary electrons are used. Elemental composition is determined by the help of back scattered electrons. Magnifying power of SEM ranges from 20X to 50000X with 50nm to 100nm resolution. The resolution of SEM is adjusted by the spot size of electron which depends on the electron wavelength. Vacuum is necessary for the working of SEM which is applied by the vacuum pumps. The sample for SEM must be conductive. The nonconductive samples are coated with very thin layer of gold or Cu.

3.2 Two Point Probe Method:

Two point probe and four point probe methods are commonly used for the measurements of resistance in conductors. By measuring the current and potential difference across the conductor we can measure the resistivity as shown in fig (3.5).

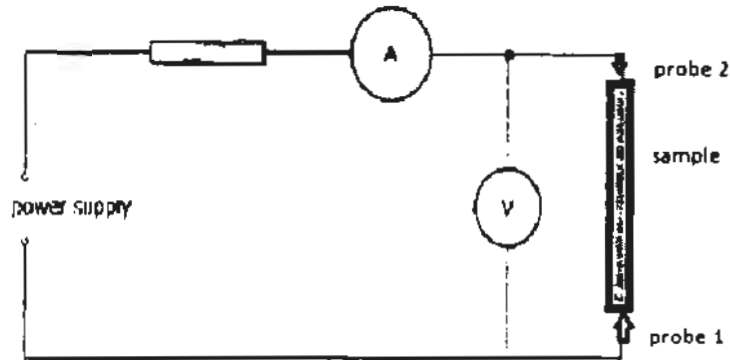


Fig 3.5: Setting of two probe system

Probe 1 is used to supply current across the sample and exit through probe 2 which is measured by ammeter. Resistivity can be measured by finding the potential difference between two probes using a voltmeter. We have the formula for resistivity as

$$\rho = \frac{V A}{I l} \quad (3.3)$$

Where l is length between probes and A is correction of sample.

3.3.1 Problems of two probe method:

- 1) "Increase in resistance due to the contact of measuring lead connection"
- 2) "It cannot be used for irregular shapes"
- 3) "It is difficult to solder some materials with lead contact like nanomaterials"
- 4) "While soldering the heating of sample like semi-conductors result in injection of impurities into material and affect the electrical property".

Four point probe is a better technique for resistivity measurements and to overcome these problems. It can be used over different shapes of sample and pressure contacts instead of soldering contacts help preventing the heating of sample.

1.8.2 The TMR effect

The MTJ consist of a very thin layer of insulator sandwiched by two FM layers. It is designed in such a way that the field for switching is different for each layer. Which concludes that each FM layer have different H_c . The layer with lower H_c is called soft layer or free layer and the other with the higher H_c is hard or pinned layer. There are a number of methods for producing H_c for the FM layers. For example to choose the FM materials having different H_c . The other is to use different shape anisotropy for the same FM layers but having difference in thickness or shape. The magnetization of one of FM layer is fixed or pinned by the exchange bias of an adjacent AFM layer is one of the most effective way to get switching at low field (as considered in practical application). The layer which is unpinned is called free layer while the pinned layer is exchange bias layer. As shown in the Fig.1.7. the dependence for the magnetization alignment of pinned and free layers on the applied field is shown in fig 1.8 (a) in which the hysteresis loops that are one which is around the zero field is from free layer contribution and other around H_{ex} is from the contribution of pinned layer due to the bias effect. H_{ex} is the exchange bias field that is produced in AFM or FM bilayer system. In fig 1.8 (b) is shown the dependence of resistance of MTJ on the magnetic field alignment of relative to the pinned and free layer. The MTJ is at low state when the magnetization of two FM layers are parallel and at high state when the magnetizations are anti parallel. TMR is defined as

$$TMR = \frac{R_{AP} - R_P}{R_P} \quad (9)$$



Fig. 1.7: Schematic illustration of MTJ consisting of free layer/Al-O or MgO/pinned layer pinned by an AFM layer.

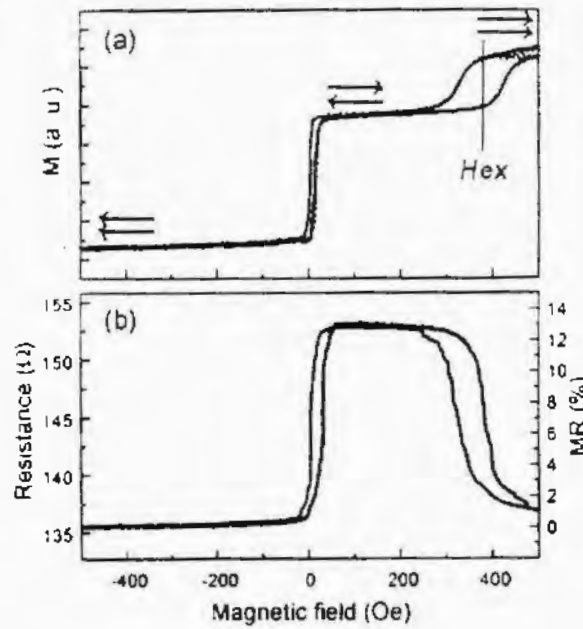


Fig. 1.8: (a)MH loop illustration of MTJ with free layer/Al-O/pinned layer pinned by AFM layer; (b) the field dependence of tunnel resistance of MTJ [33].

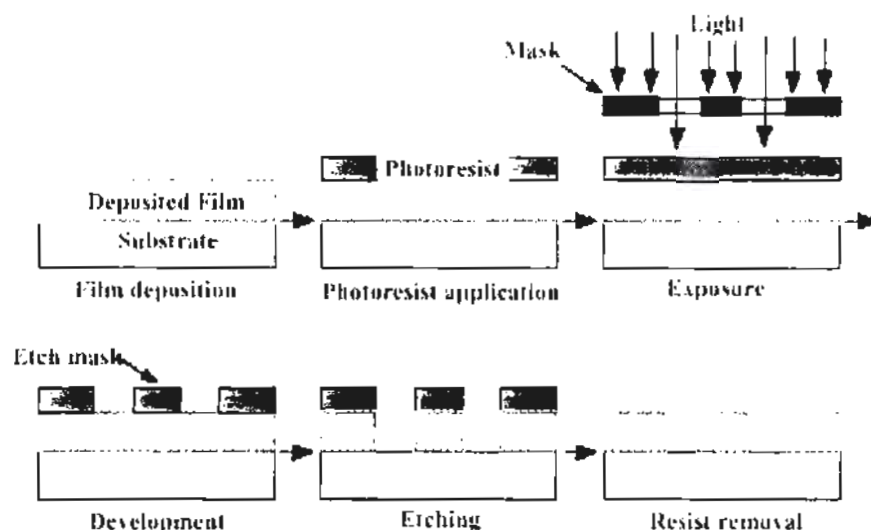


Fig. 2.4: Diagram representation of three stages involved in photolithography.

First the organic photoresist is coated on the cleaned film and is allowed to dry. Then the UV light is exposed on film to form a geometrical pattern through the mask (fig 2.4a). Secondly the part of photo resist which is exposed to the UV light is removed because it becomes unstable, it is developed in the photo resist developer for optimized time (fig 2.4b), unexposed film is removed by etching after doing the pattern [52-53]. In last the photo resist remained is removed by dipping in to solvent suitable for that purpose (fig 2.4c).

2.1.3 Ion-beam etching:

It is a dry etching process in which momentum is transferred between the incident ion and target atom. Argon ion with sufficient energy are radiated on the surface. These argon ions with sufficient energy help to eject the material from the surface. A vacuum pump exhausts the ejected material and gases to avoid any deposition on the sample. Sputtering yield depends on the incident ion energy, mass of species, target atom mass and angle of incidence [54-56]. The energy of the incident atom must be greater than the binding energy of the target atoms it could range from 10 to 100 KV depending on the material. Etching rate(R) is a function of sputtering yield(S) and written as

$$R(\theta) = 9.6 \times 10^{25} \times J \times (S(\theta)/n) \times \cos(\theta) \quad (2.2)$$

Where J is current density, n is atomic number density and (θ) is the angle of incident with normal

2.5 Electro deposition Technique

Deposition of material by passing current between two electrodes which are placed in some electrolytic solution is called electrodeposition. This technique is most commonly used for the growth of nano wires with high aspect ratio and also for the thin film growth. It is convenient and low cost as well. It is considered more beneficial over the physical method because it is easier to handle and has high deposition rates, it also does not require any vacuum for its working and uniform films can be easily grown. We can grow a variety of materials including metals, alloys and metal matrix compounds. NWs and thin films are included in materials fabricated electrochemically. The current distribution is better to be known on the electrode to design the best device suitable for the generation of required items because metals and alloys are fabricated by ED. There are a number of parameters which should be taken in to account to have the best deposition. These are as follow.

- Electrolyte concentration
- Current density
- pH
- buffer capacity
- leveling agents
- temperature
- substrate properties
- contaminants
- cleaning procedure

The process of electrodeposition is illustrated in the fig. the structure and deposition depends on these parameters. In this work we have used electrodeposition technique for the fabrication of thin film on home-made AAO templates.

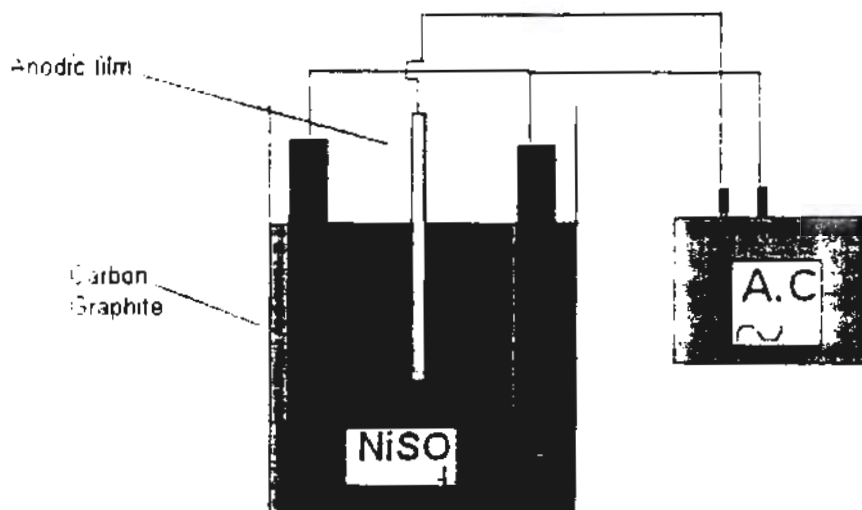


Fig 2.5: illustration of Electrodeposition process.

2.5.1 Template assisted electrochemical deposition

Electrochemical deposition is a versatile and low cost effective technique for the fabrication of nanostructures. We require AAO or polycarbonate templates for this process. Both membranes can be easily found commercially and can also be prepared in the laboratory.

2.5.2 Types of Electrodeposition

There are three main types of ECD for the NW and thin film growth which are

1. Alternating current electrodeposition (ACECD) [57 58]
2. Direct current (DC) electrodeposition
3. Pulse current electrodeposition

The AAO templates are mainly prepared by DC voltage between Al electrodes. In DC method a direct current is applied through-hole AAO that is isolated from Al substrate. Also a conductive film should be sputtered on one side of the templates before the start of deposition. We require only a few nm thick AAO templates for nanostructure application. However, it is better to use 20µm thick templates for easy handling and transfer. In AC and PED methods metal NW and thin film can easily be deposited directly into pores of AAO templates with Al substrate. AC method is considered as the most convenient and popular method for the fabrication of NW and thin film [59].



Fig. 1.7: Schematic illustration of MTJ consisting of free layer/Al-O or MgO/pinned layer pinned by an AFM layer.

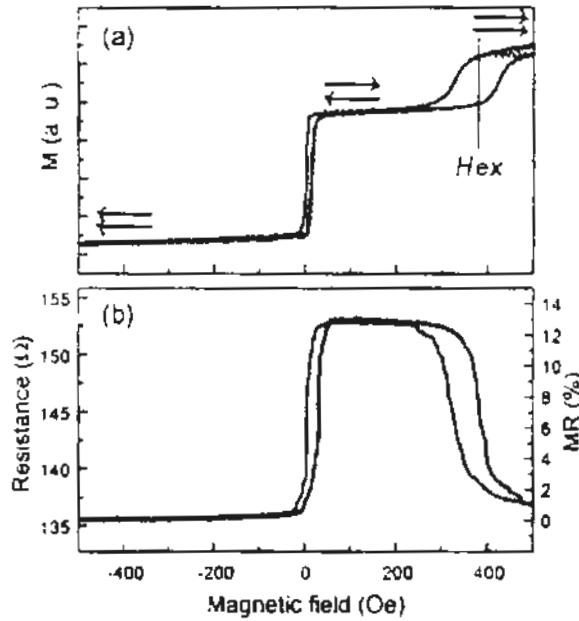


Fig. 1.8: (a) MH loop illustration of MTJ with free layer/Al-O/pinned layer pinned by AFM layer; (b) the field dependence of tunnel resistance of MTJ [33].

(TMR) data for the free layer hysteresis in a typical MTJ with an AlO_x tunnel barrier

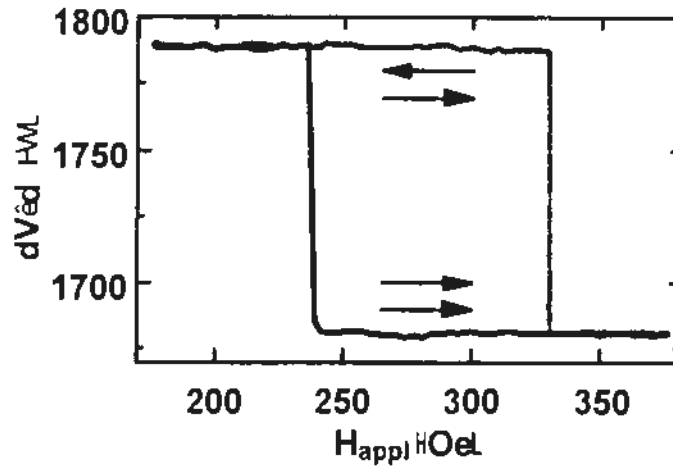


Figure 1.9: Plot of differential resistance vs. H_{app} for the free layer hysteresis of a typical AlO_x MTJ.

Figure 1.9 gives an example of tunnel magnetoresistance

1.9 Spin-Transfer Torque (STT) Domain Wall Motion

The spin of electron becomes polarized in the direction of magnetization (e.g., spin up or spin down) when it passes through a magnetized material (fig 1.10). When these spin polarized electrons reaches a region of different orientation of magnetization, as in domain wall, to align with the magnetization, its spin is again polarized. This re alignment of spin results in an electron angular momentum. A torque is exerted on the local magnetic moment of the magnetic material to conserve this angular momentum. To align it with the initial polarization of electron this spin transfer torque acts on the magnetization [34 35].for example the spin transfer torque will act to pull the magnetization down if an electron with spin down enters in an up orientation magnetization region. For the movement of domain walls in direction of electron flow this phenomenon can be used in magnetic materials. This phenomenon has been used in racetrack memory [36] and in various magnetic memories to drive the switching. It is also used for the switching single domain pillar MRAM [37].

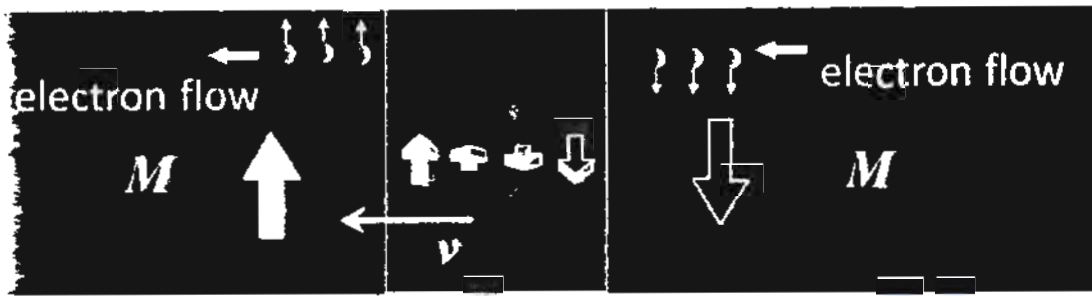


Figure 1.10 Illustration of spin-transfer torque-driven domain wall motion. The domain wall moves in the direction of the electron flow.

Let's consider a sample slice having thickness dx , in the direction of current flow (one dimensional). The time rate of change of spin angular momentum or spin torque can be calculated by equating the time evolution of the local magnetization and amount of the angular momentum deposited by spin polarized conduction electrons.

$$\frac{dS^z}{dt} = -\frac{1}{\gamma} \frac{\partial \mu^z}{\partial t} = -\frac{1}{\gamma} \frac{\partial M^z}{\partial t} dx dy dz = P \left(\frac{-e}{2} \right) \frac{\hbar}{2} dy dz \left[\frac{M^z(x+dx) - M^z(x)}{M_s} \right] \quad (9)$$

Here, μ^z is the magnetic moment, M_s the saturation magnetization of the material, γ the gyromagnetic ratio (equal to $\frac{g\mu_B}{\hbar}$, where g is the Landé factor and μ_B the Bohr magneton), P the electron spin polarization, J the charge current density, e the electron charge, \hbar the reduced Planck constant, and M^z the magnetization vector. The resulting time rate of change of the magnetization due to the spin current is obtained by solving the above equation for $\frac{\partial \vec{M}}{\partial t}$:

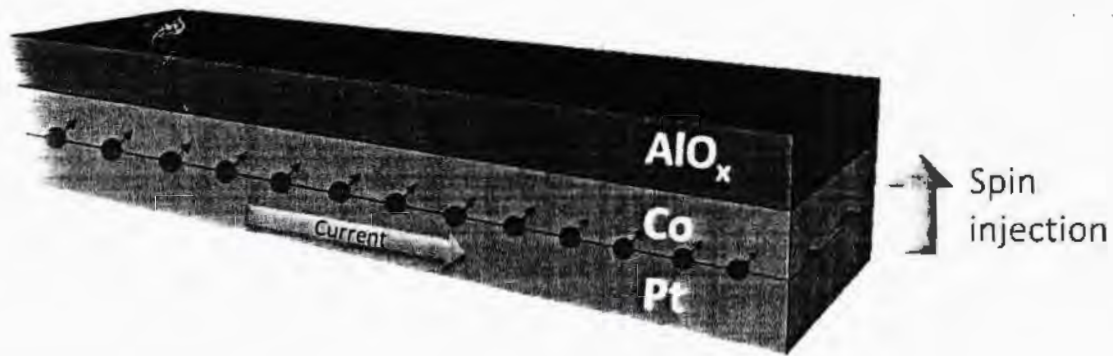


Figure 1.11: – Illustration of spin injection from Pt to Co due to the spin Hall Effect in a Pt/Co/AIO_x structure.

It could be expected initially that this in plane spin injection has the ability to sustain the motion of perpendicular domain wall. For instance, if the structure of the domain wall is to be Néel form, with a wall center which is orthogonal to the spins injected and along the length of wire, the domain wall can be moved. As shown in the fig 1.12. Suppose that domain wall has chirality shown, in such a way that the central moment of the wall is the direction $-\hat{x}$. If the flow of electron is in the $+\hat{x}$ -direction, the spins that are aligned along $-\hat{y}$ will be injected from the Pt into the magnetic layer. The domain wall will be moved along the direction of the current flow.

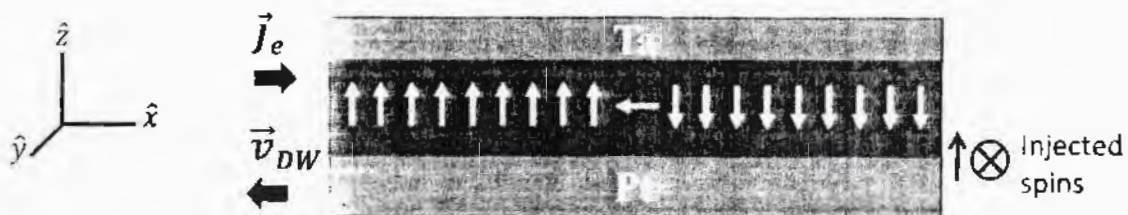


Figure 1.12: – Illustration of scenario in which in-plane spins injected by the SHE move a domain wall with Néel structure opposite the electron flow.

It should be noted that as the domain walls are aligned at 90° to the wall center, the spins injected create a torque that drives the domain wall. No torque would result and the two moments would be either parallel or antiparallel if the walls were Bloch type. Bloch wall are normally preferred

because Neel walls are unfavorable due to internal demagnetization energy associated to them. [40]. However, additional force that is Dzyaloshinskii-Moriya interaction (DMI) is found to dominate in some cases. [41-44]. This effect tends to produce stable Neel walls which are suitable for moving with the spin hall effect (SHE). Domain wall motion with high velocity has been demonstrated experimentally in these systems [40-44]. We can set the way in which domain walls moves with response to the current by reversing the chirality. In other words it is possible to flow the electron along SHE-DWM if DMI or some external field sets the wall chirality in the correct direction.

CHAPTER 2 Synthesis and Fabrication

2.1 Synthesis of Nanomaterials

In this chapter the synthesis techniques adopted for the sample preparation and device fabrication are explained. In general the two common techniques used for the synthesis are top down and bottom up approaches as explained below.

2.2 Top-down and Bottom-up approach:

When we synthesize the nano materials by machining or crushing the bulk material this type of approach is called top down approach. For example the manufacturing of integrated circuits by crystal growth, lithography, ion beam etching etc. the most common example for the synthesis of nano materials is ball milling process. In this process the microcrystalline structures are broken without disturbing the integrity of the material in to nano crystalline materials. Kinetic energy is supplied for the preparation of the nanostructure metal oxide by chemical reaction between the constituents in crushing by milling process.

In contrast, the assembly of materials by the atoms or molecules to form the nano materials is called bottom up approach. It is a non-lithographic technique having great potential to overcome the lithographic process. Sol gel, PVD, CVD, laser ablation, electrodeposition, epitaxial growth etc. are examples of bottom up approach.

2.3 Sputtering:

Sputtering is a PVD process in which we can deposit thin films and multilayers on substrates. In this process highly energetic particle which could be electron, an ion or an alpha particle etc. are targeted on the surface of the material to be deposited the incident particles must have enough energy to eject the surface atoms. The sputtered atoms are deposited on the substrate. The ratio of number of atoms ejected to the incident atoms is called sputter yield.

2.3.1 DC diode sputtering:

DC sputtering is a process in which the discharge occurs between target and substrate under suitable conditions of voltage and pressure. A neutral gas at low pressure is inserted in to the vacuum chamber. A discharge under suitable pressure (1 to 10m torr) and voltage conditions occurs between target and substrate in DC diode sputtering. Argon gas which is electrically neutral is inserted in low pressure vacuum chamber. Argon gas is ionized in to plasma by the DC voltage

between substrate and target resulting into ions and electrons. The charged ions are accelerated towards the target which is anode. The ions hit the target at high speed and eject the atoms from target. The atoms sputtered after this process are deposited on the substrate which is cathode. As a result we get a thin film of required material. More argon ions and electrons are produced by the collision of prior ionized ions of argon when they are accelerated towards anode. The required voltage applied for discharging is a function of pressure and spacing between electrodes [45] fig 2.1 shows the mechanism of DC diode sputtering. It is normally operated at high pressure to increase the ionization and electron impact in the chamber. The drawback of high pressure is poor transport and low deposition rate of atoms.

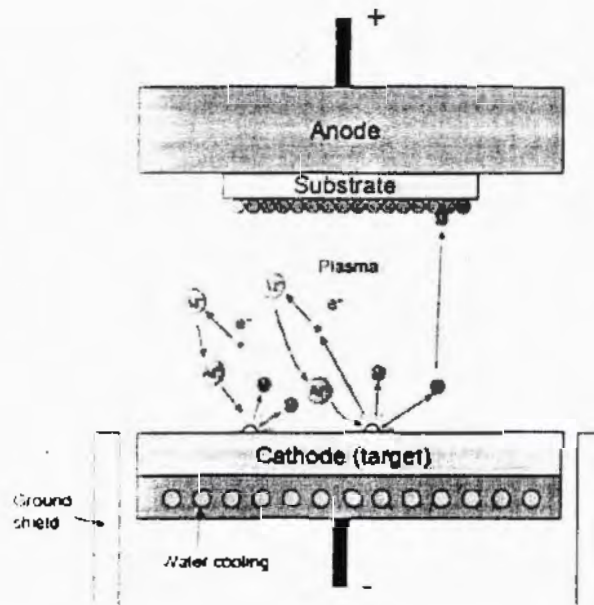


Fig.2.1: Structure of basic DC diode sputtering system.

2.3.2 RF diode sputtering:

Alternate voltage is applied between the electrodes to resolve the problem occurred in DC sputtering. Increased ion current density and elimination of charging of isolated cathode is achieved by this method. The AC frequency used is often 13.56 MHz in RF sputtering. Electrons in plasma pick more energy by the plasma oscillation at this frequency, resulting into electron population and more ionization. Higher ionization result in high ion current at the same power applied as in DC sputtering. Another benefit of RF diode sputtering is that cathode doesn't gain charge from plasma by the switching of anode and cathode. Figure 2.2 describe the structure of RF sputtering system.

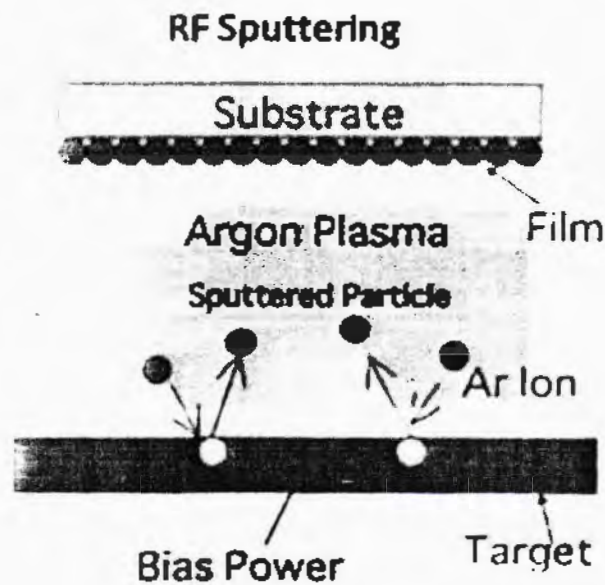


Fig 2.2: Basic structure of RF sputtering system.

2.3.3 Magnetron sputtering:

Magnetron sputtering is commonly used for the synthesis of multilayer thin films. Magnetron sputtering uses the relation of electron response to magnetic field.

$$F = e (V \times B) \quad (2.1)$$

Here e is charge of electron, V velocity and B is magnetic field. F is force that makes the electron move around the magnetic field which increases the impact probability with atoms of gas to cause the ionization. In turn producing the high densities of plasma and low discharge voltage at constant power [45-51]. The magnetron sputtering system is a chamber placed in vacuum. Sputtering up or sputtering down are two main types of chambers. The vacuum chamber has a cathode plate and an anode which is cylindrical. The substrate is placed in to the chamber with argon gas inserted at constant rate. Magnets which are placed under the target produce strong magnetic field to help deposition at confined place at substrate. Plasma is formed by the highly ionized gas. In the mean while the electrons ejected from the target interact with the argon gas to produce positive ions of argon. These ions strike with the cathode target and remove the atoms from it which are moved to the substrate and stick on it to form thin film as shown in fig 2.3

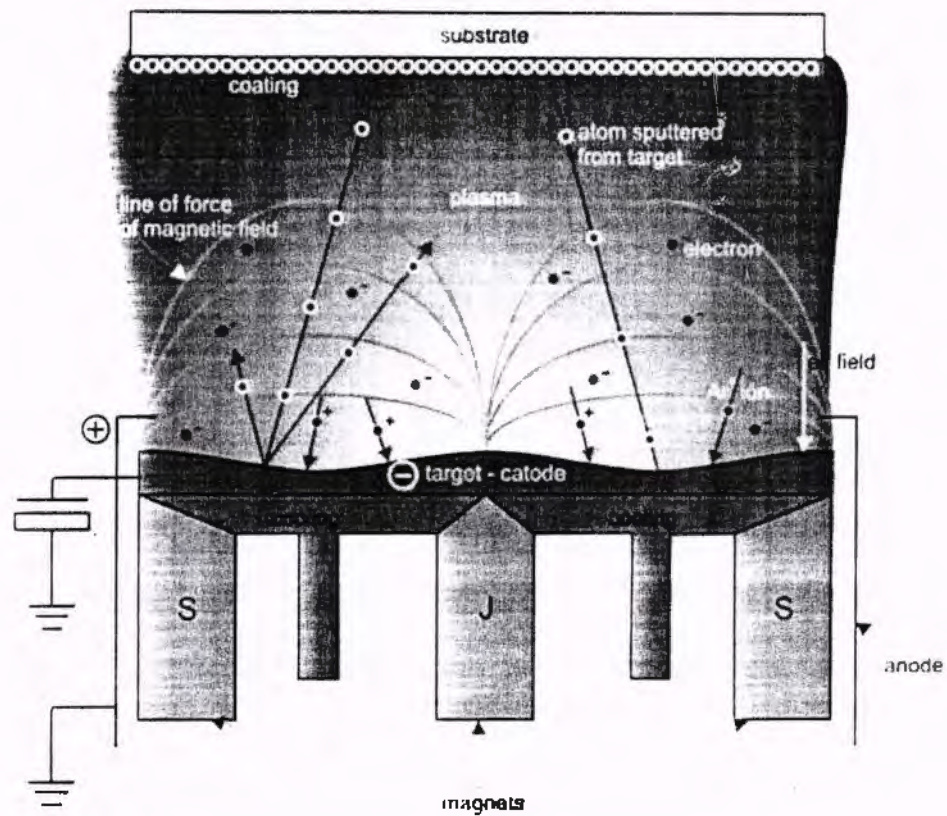


Fig.2.3: Showing Basic components of Magnetron sputtering system.

The heating of substrate up to high temperature 900C is avoided by the rotation of substrate with RF and DC bias. Automatic chamber pumping is provided by the computer controlled electro pneumatic valve and dry backing pump. All the parameters are monitored by lab view software. Both single and multiple sources for deposition can be used depending upon material sputtering efficiency.

2.4 UV Lithography:

Removing a selective part of a film or bulk material using UV rays is called UV or photo lithography. A geometrical pattern of light is incident upon the light sensitive photo resist using a photo mask, the resist is then etched by the chemical or physical method from substrate. There are two types of mask lithography used with coherent light one is contact and other is projection lithography. The mask is placed very close to the substrate to remove the selected film in contact lithography. It help us to go below the limit of wavelength with the accurate distance between the mask and film it also helps to pass the wave through the hole smaller than the wavelength applied. The figure below explains the patterning by photolithography.

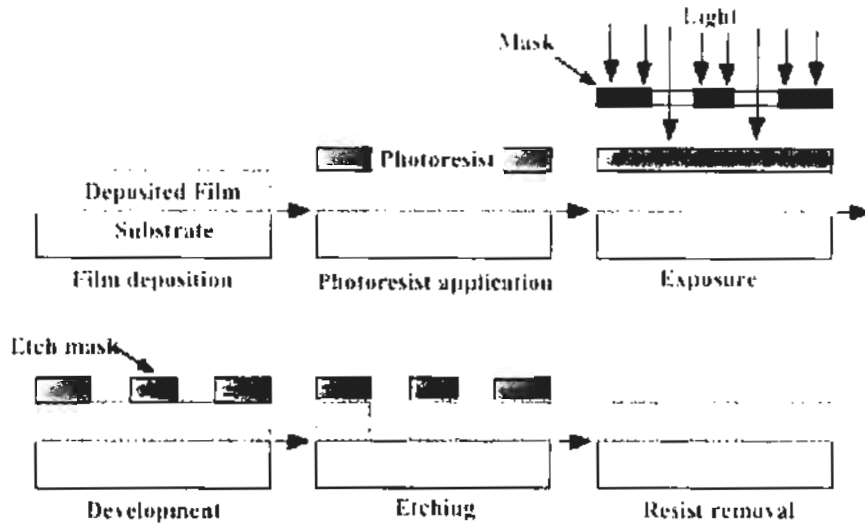


Fig. 2.4: Diagram representation of three stages involved in photolithography.

First the organic photoresist is coated on the cleaned film and is allowed to dry. Then the UV light is exposed on film to form a geometrical pattern through the mask (fig 2.4a). Secondly the part of photo resist which is exposed to the UV light is removed because it becomes unstable, it is developed in the photo resist developer for optimized time (fig 2.4b), the unexposed film is removed by etching after doing the pattern [52-53]. In last the photo resist remained is removed by dipping in to solvent suitable for that purpose (fig 2.4c).

2.3 Ion-beam etching:

It is a dry etching process in which momentum is transferred between the incident ion and target atom. Argon ion with sufficient energy are radiated on the surface. These argon ions with sufficient energy help to eject the material from the surface. A vacuum pump exhausts the ejected material and gases to avoid any deposition on the sample. Sputtering yield depends on the incident ion energy, mass of species, target atom mass and angle of incidence [54-56]. The energy of the incident atom must be greater than the binding energy of the target atoms it could range from 10 to 100 KV depending on the material. Etching rate(R) is a function of sputtering yield(S) and written as

$$R(\theta) = 9.6 \times 10^{25} \times J \times (S(\theta)/n) \times \cos(\theta) \quad (2.2)$$

Where J is current density, n is atomic number density and (θ) is the angle of incident with normal

2.6 Electro deposition Technique

Deposition of material by passing current between two electrodes which are placed in some electrolytic solution is called electrodeposition. This technique is most commonly used for the growth of nano wires with high aspect ratio and also for the thin film growth. It is convenient and low cost as well. It is considered more beneficial over the physical method because it is easier to handle and has high deposition rates, it also does not require any vacuum for its working and uniform films can be easily grown. We can grow a variety of materials including metals, alloys and metal matrix compounds. NWs and thin films are included in materials fabricated electrochemically. The current distribution is better to be known on the electrode to design the best device suitable for the generation of required items because metals and alloys are fabricated by ED. There are a number of parameters which should be taken in to account to have the best deposition. These are as follow.

- Electrolyte concentration
- Current density
- pH
- buffer capacity
- leveling agents
- temperature
- substrate properties
- contaminants
- cleaning procedure

The process of electrodeposition is illustrated in the fig. the structure and deposition depends on these parameters. In this work we have used electrodeposition technique for the fabrication of thin film on home-made AAO templates.

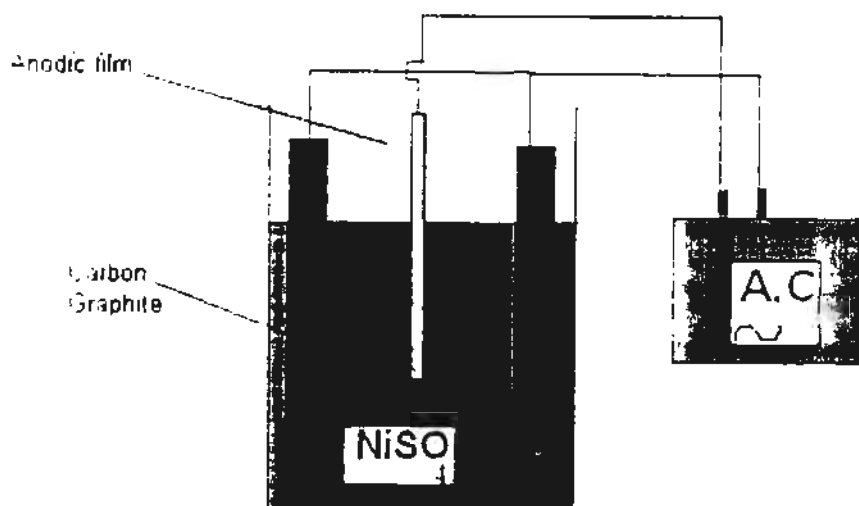


Fig 2.5: illustration of Electrodeposition process.

2.5.1 Template assisted electrochemical deposition

Electrochemical deposition is a versatile and low cost effective technique for the fabrication of nanostructures. We require AAO or polycarbonate templates for this process. Both membranes can be easily found commercially and can also be prepared in the laboratory.

2.5.2 Types of Electrodeposition

There are three main types of ECD for the NW and thin film growth which are

1. Alternating current electrodeposition (ACECD) [57 58]
2. Direct current (DC) electrodeposition
3. Pulse current electrodeposition

The AAO templates are mainly prepared by DC voltage between Al electrodes. In DC method a direct current is applied through-hole AAO that is isolated from Al substrate. Also a conductive film should be sputtered on one side of the templates before the start of deposition. We require only a few nm thick AAO templates for nanostructure application. However, it is better to use 20 μ m thick templates for easy handling and transfer. In AC and PED methods metal NW and thin film can easily be deposited directly into pores of AAO templates with Al substrate. AC method is considered as the most convenient and popular method for the fabrication of NW and thin film [59].

2.7 CoFeB /Al-O/ CoFeB/Al-O/CoFeB Double barrier magnetic tunnel junctions:

The DBMTJ's are composed by two tunneling barriers around an intermediate layer of ferromagnetic material, this type of magnetic tunneling junction could gain new properties. The two magnetic layers have different switching fields due to different coercivity. Free layer is the layer with low coercivity and the other with high coercivity is the fixed layer. We can change the orientation of the free layer by applying low field which gives it the operation of memory device. To avoid the permanent change of orientation of domains in pinned layer due to exchange coupling effect, pinned layer is coupled with anti-ferromagnetic material. The moment of ferromagnetic layers is coupled with nonmagnetic bias and exchange in opposite direction by the synthetic antiferromagnetic layer of CoFe/Ru/CoFe/IrMn and pinned layer is produced by adjustment of Ru thickness.

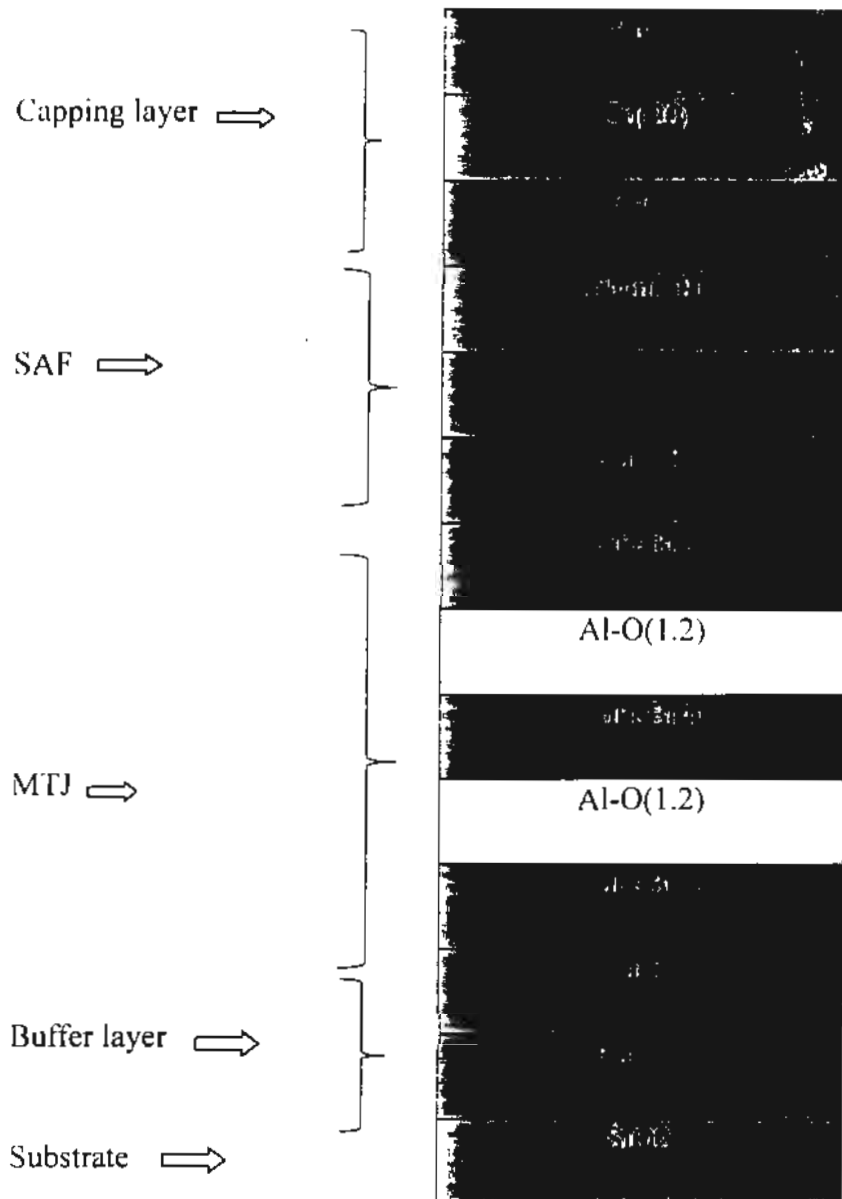


Fig 2.6: Diagram represents multilayer stack of DBMTJ

The huge tunneling spin polarization, high anisotropy and soft magnetic behavior of CoFeB makes it the best candidate for synthesis of MTJ which was employed in our work. We have used AlO as the insulating barrier in this MTJ. The mobility of s-type electrons is increased by the interaction of transition electrodes and insulating barrier which leads to the spin current in MTJ [66-67]

2.8 Fabrication of Magnetic Tunnel Junction:

The steps for the fabrication of MTJ are given below it was done by top down method.

2.3.1 Step 1: Fabrication of bottom electrode

- i) Bottom electrodes were pattern by pasting positive resistor.
- ii) Uniform resist was distributed by spin the sample for optimized time
- iii) More uniformity was got and impurities were removed by baking the sample for 1 min at 90C.
- iv) Resistor is paste on the desired part by UV mask lithography.
- v) Resistor becomes unstable when it is exposed to the UV light having suitable wavelength it was removed by developing in photo developer for 35 to 40 sec and 20 to 25 sec in water.
- vi) Films uncovered by resist were removed by etching.
- vii) To remove the resistor, sample was dipped in to acetone after etching
- viii) Bottom electrode was composed after the first step

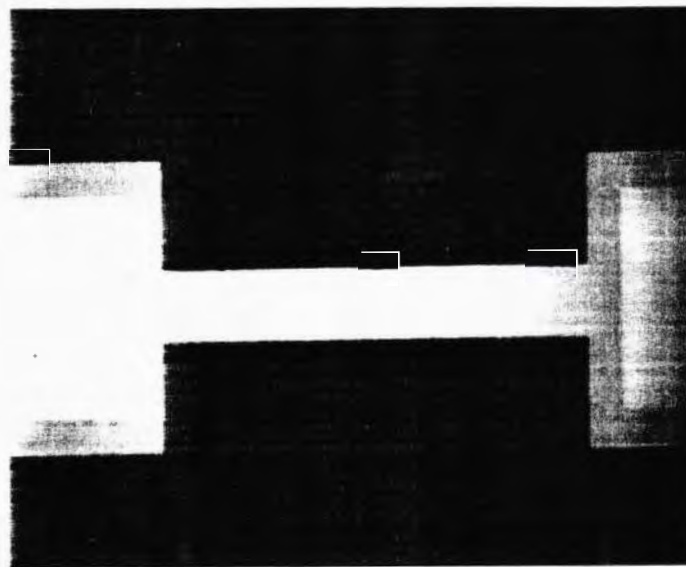


Fig: 2.7 Shows the fabricated bottom electrode. [69]

3.2 Step 2: Fabrication of tunnel junction:

The negative resistor was pasted on the sample and MTJ was fabricated. The resistor became unstable by exposing to UV light and was then removed by etching. As shown SiO₂ was deposited on sample.

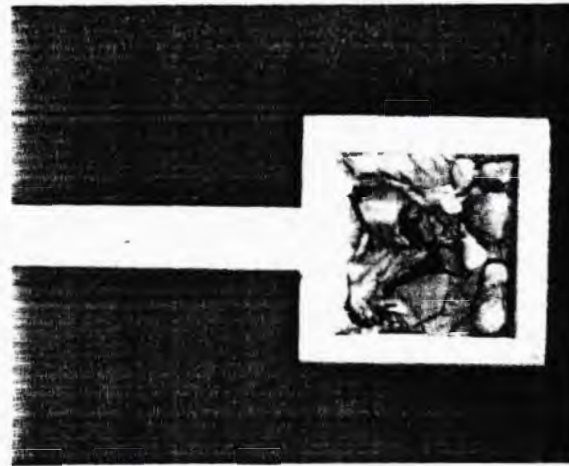
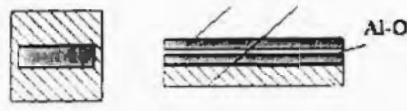
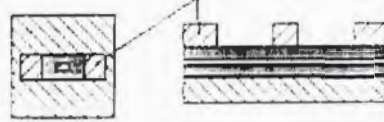

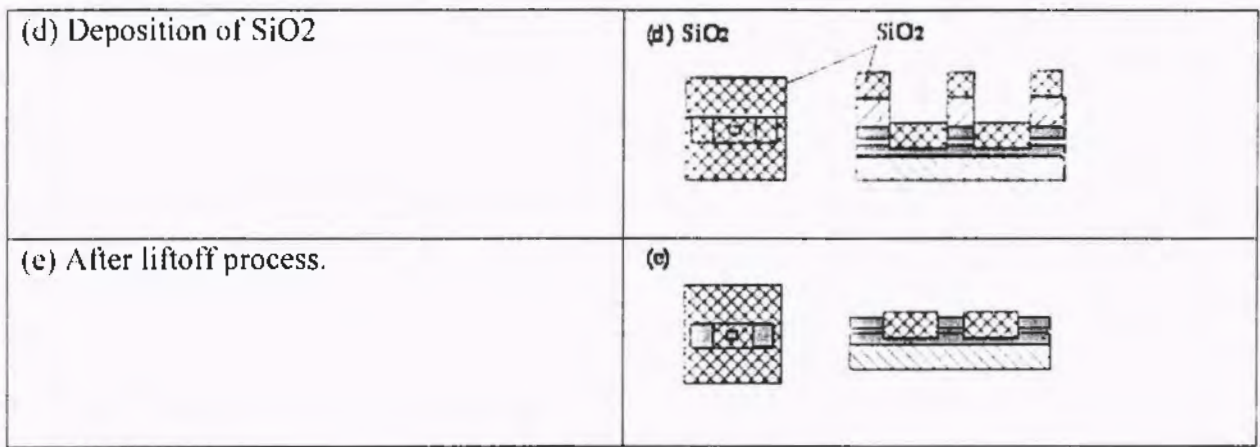


Fig 2.8 Appearance of SiO₂ depositions on the sample [69]

All the above stages are described in table 2.1

Table 2.1 Stages of fabrication [69]

(a) Multilayers on substrate.	<p>(a)</p>  <p>Magnetic films Al-O</p>
(b) Sample after UV lithography.	<p>(b)</p>  <p>Resistor</p>
(c) Etching process.	<p>(c)</p>  <p>Ar ion etching</p>



2.3.3 Step 5: Fabrication of Top Electrode:

Cu is deposited to form top electrode as step 1 after the removal of unnecessary SiO₂.

- i) Positive resistor is pasted on sample to pattern top electrode.
- ii) UV mask lithography is used to paste strongly the resistor on the desired part so that it is protected during etching process.
- iii) Etching is used to remove unnecessary film, which are uncovered by the resistor.
- iv) After etching the sample is dipped in acetone and put in ultrasonic bath for some time in order to remove the resistor.

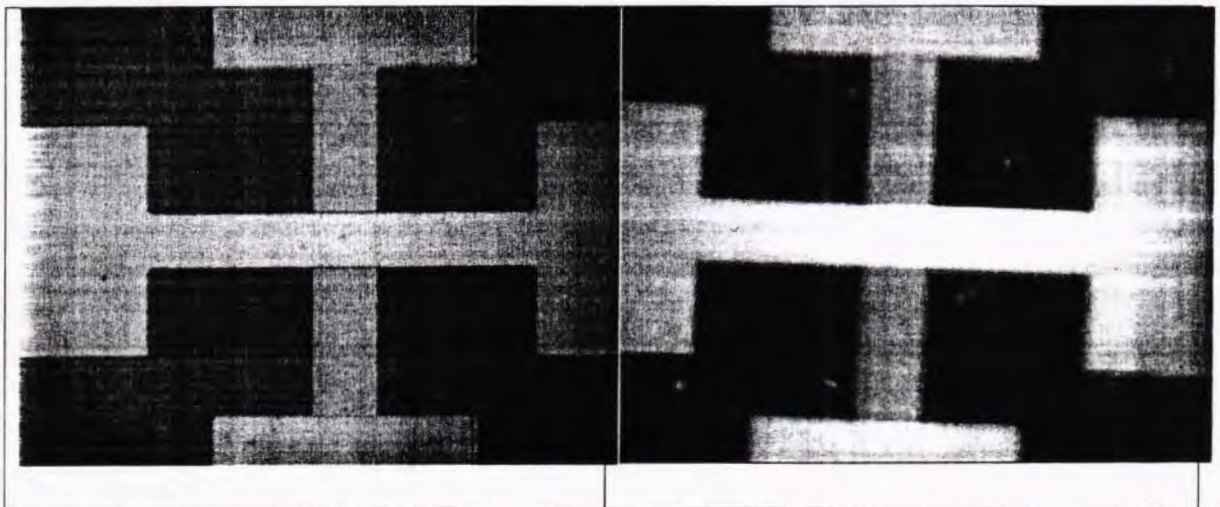


Fig 2.9 (a) left shows sample before dipped in acetone. (b) Right shows sample after dipped in acetone [69]

2.4 Fabrication of CoFeB thin film

Thin film of CoFeB was deposited on home-made AAO templates. The fabrication process was carried out in the Spintronics lab IITUI. First of all AAO templates were prepared on Al substrate by the following steps

- Electro-polishing of Al Foil
- First step Anodization
- Heat treatment
- Second step Anodization
- Breaking of barrier layer
- Removal of Remaining Al Foil
- Opening of the Pores

The electrolyte solution for the film deposition was prepared using CoSO_4 for Co source, $\text{FeO}_4\text{S}7\text{H}_2\text{O}$ for Fe source and H_3BO_3 for B source. Solution was prepared using 0.025M CoSO_4 , 0.0054M $\text{FeO}_4\text{S}7\text{H}_2\text{O}$ and 0.2M H_3BO_3 . The solution pH was 4.5 and 0.02gm ascorbic acid was mixed in solution to prevent the oxidation due to the presence of Fe.

Thin film of CoFeB was deposited by electrodeposition at room temperature for 5 min at 15V.



Fig. 2.10 (a) Electrodeposited film of CoFeB

(b) Electrolytic solution

The thin films were deposited under following conditions given in the table 2.2.

Table 2.2 Conditions for CoFeB thin film preparation.

Sample no.	Material deposited	Voltage (V) applied	Time (min) of deposition	PH of sol.	Concentration in 100 ml		
					CoSo4	FeO4S7H2O	H3Bo3
1	CoFeB	15	5	4.5	0.025 M	0.05 M	0.2 M
2	CoFeB	15	6	4.5	0.025 M	0.05 M	0.2 M
3	CoFeB	15	7	4.5	0.025 M	0.05 M	0.2 M
4	CoFeB	15	8	4.5	0.025 M	0.05 M	0.2 M
5	CoFeB	15	9	4.5	0.025 M	0.05 M	0.2 M
6	CoFeB	15	10	4.5	0.025 M	0.05 M	0.2 M

The thickness of the films is varied by changing the time of deposition. The effect of thickness variation is studied and the detailed analysis of magnetic properties variation and Hall Effect occurrence is given in corresponding headings.

CHAPTER 3 Experimental Techniques

3.1 X-Ray Diffraction (XRD):

Lattice is the building block that all materials have, lattice have two or three dimensions. The interatomic length and three interfacial angles of lattice are shown in the fig. Crystals have regular arrangement of lattice which is repeated. XRD peaks are obtained by the regular and repeated arrangement of the lattice.

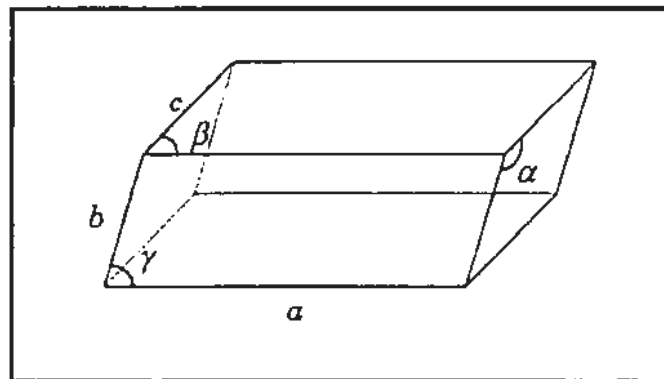


Fig 3.1: Geometrical shape of lattice with angles and lengths

The arrangement of molecules and atoms in crystal structure are found by diffraction process. The X-ray beam of suitable wave length gives the information of crystal structure by scattering back from sample after incidence. Bonding and other parameters are found by this beam of X-ray. We get the information about crystal and amorphous nature of material by diffraction method. Bond length, atomic spacing and particle size can be found by crystallographic method. The process of diffraction is used to study DNA structure, proteins and vitamins. There are different methods for X-ray diffraction. The X-rays produced for diffraction must have wavelength equal to the interatomic spacing.

3.1.1 Production of X-rays:

A German physicist named Roentgen discovered X-rays. By X-rays we can find the crystallographic nature of material, nature and bonding composition, lattice parameters, and orientation of crystals, grain size and defects in materials. Diffraction technique can be applied on both bulk and nano levels.

Thermionic emission of electrons occurs by a heavy target like tungsten when a beam of electrons produced by the filament strikes the target Fig.3.2. [61]

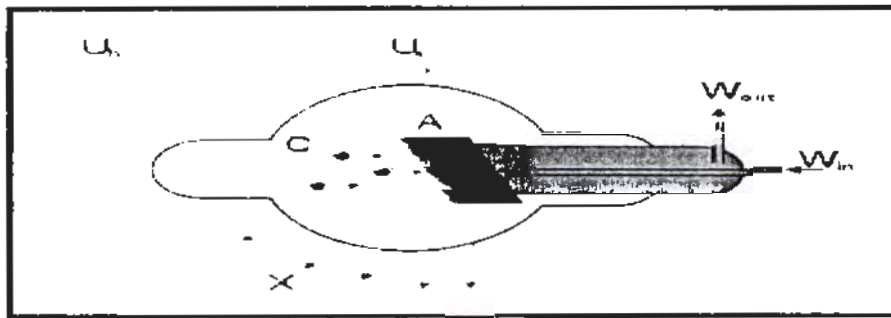


Fig.3.2:X-ray cooling tube

For this purpose cooling tube is used. X-rays are electromagnetic in nature having wavelength from 0.5 \AA to 2.5 \AA . This value of wavelength is equal to wavelength in solid materials [63]. X-ray diffractometer works on principles of Bragg's law.

3.1.2. Bragg's Law:

Monochromatic beam of X-ray with suitable wavelength falls on the target and scatters in different directions after interacting with the material atoms. Diffraction of X-ray is known as scattering of x-rays in preferred directions by the crystalline material. By determining the "d spacing" of material we can analyze the crystal structure of material with the help of diffracted x-rays directions.

Bragg law is given by.

$$2d\sin\theta = m\lambda \quad (3.1)$$

Where,

m = fringe order 1, 2, 3.....

λ = wavelength of beam of X-rays

d = spacing between planes,

θ = angle between plane and beam of light

Experimental arrangement of Bragg's Law as shown in Fig. 3.3

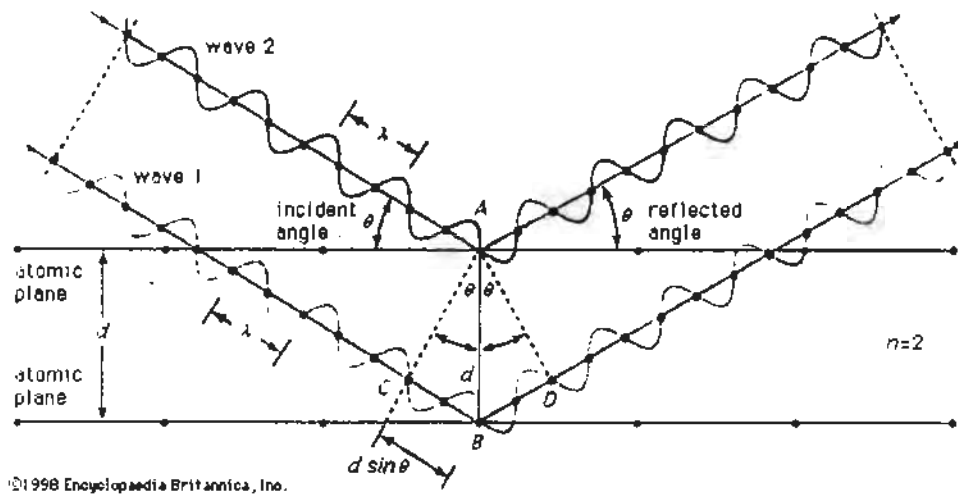


Fig.3.3: Experimental arrangement of the Bragg Law

For cubical spinel structure the lattice parameter a can be calculated by formula

$$a = d / \sqrt{(h^2 + k^2 + l^2)} \quad \text{—————} \quad (3.2)$$

Where h, k, l are called miller indices.

3.2. Scanning Electron Microscopy:

For detailed structural analysis SEM is an important characterization method. By scanning electron microscopy we can find the particle size, structure, grain size and surface can be analyzed. SEM show the direct image of material which is the main advantage of SEM over XRD. It is similar to the optical microscopy. A beam of electrons is produced by a filament or an electron tunneling source. These emitted electrons gain kinetic energy by high electric fields which are used to control the movement of thee electrons. The beam of electrons passes through several lenses to get a highly focused beam on the target. There are two main type of microscopies used that are SEM and TEM. SEM is used for the three dimensional image of very high resolution which is helpful to understand the morphology of the material. The beam of electrons emitted from the sample is studied with the help of detectors after amplification. Some of the electrons are back scattered and some secondary electrons are also emitted which gives important information about the sample. The surface of SEM is grounded to avoid any distortion. Fig. 3. 4 shows schematic diagram of SEM.

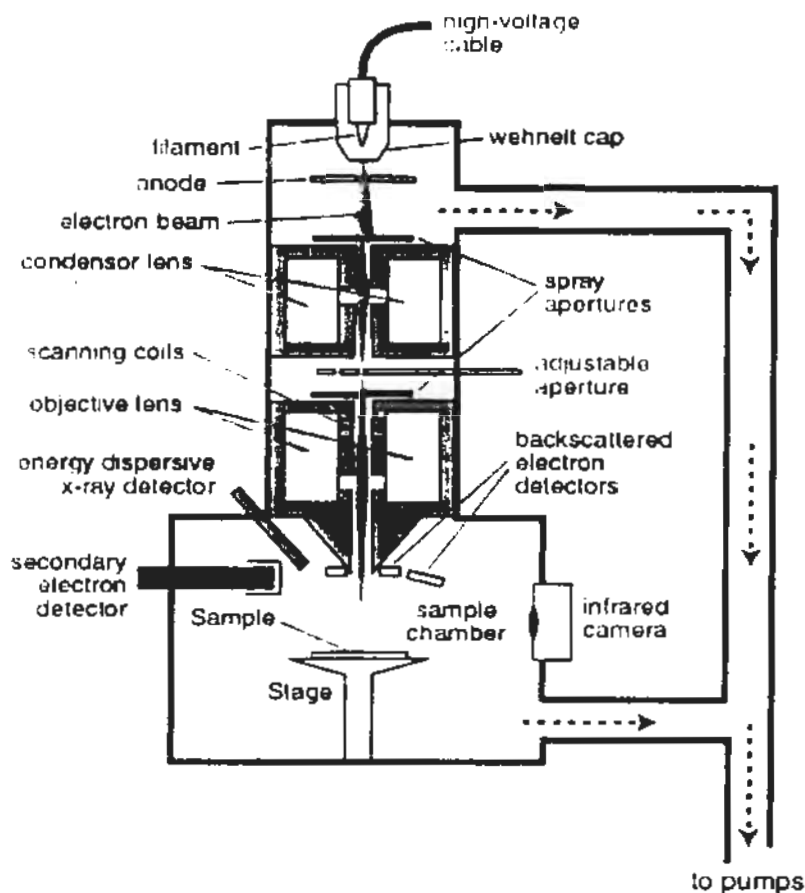


Fig. 3.4: Schematic diagram of Scanning electron microscope

Different parts used in SEM are heating filaments conducting lenses, objective lenses, electron gun and aperture. Electron gun emits the electrons which are accelerated through gaining KE by applying high voltage of 100eV to 100 KeV between anode and filament. Verity of pulses of signals are produced by the emitted electrons when they gain KE.

Backscattered electrons, diffracted electrons, secondary electrons, heat, visible light and photons are parts of these pulses of signals. For sample imaging back scattered and secondary electrons are used. For topography and surface morphology secondary electrons are used. Elemental composition is determined by the help of back scattered electrons. Magnifying power of SEM ranges from 20X to 50000X with 50nm to 100nm resolution. The resolution of SEM is adjusted by the spot size of electron which depends on the electron wavelength. Vacuum is necessary for the working of SEM which is applied by the vacuum pumps. The sample for SEM must be conductive. The nonconductive samples are coated with very thin layer of gold or Cu.

3.3 Two Point Probe Method:

Two point probe and four point probe methods are commonly used for the measurements of resistance in conductors. By measuring the current and potential difference across the conductor we can measure the resistivity as shown in fig (3.5).

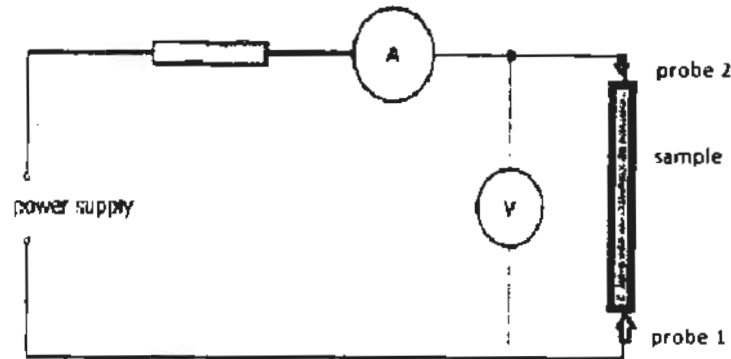


Fig 3.5: Setting of two probe system

Probe 1 is used to supply current across the sample and exit through probe 2 which is measured by ammeter. Resistivity can be measured by finding the potential difference between two probes using a voltmeter. We have the formula for resistivity as

$$\rho = \frac{V A}{I l} \quad (3.3)$$

Where l is length between probes and A is correction of sample.

3.3.1 Problems of two probe method:

- 1) "Increase in resistance due to the contact of measuring lead connection"
- 2) "It cannot be used for irregular shapes"
- 3) "It is difficult to solder some materials with lead contact like nanomaterials"
- 4) "While soldering the heating of sample like semi-conductors result in injection of impurities into material and affect the electrical property".

Four point probe is a better technique for resistivity measurements and to overcome these problems. It can be used over different shapes of sample and pressure contacts instead of soldering contacts help preventing the heating of sample.

3.4. Four point probe method:

Tungsten metal tips with spring supports having finite radius are used in this technique. They are spaced equally as shown in the fig (3.6). Springs prevent any damage to the sample by not pressing too hard on it and they can move up and down according to surface while characterization.

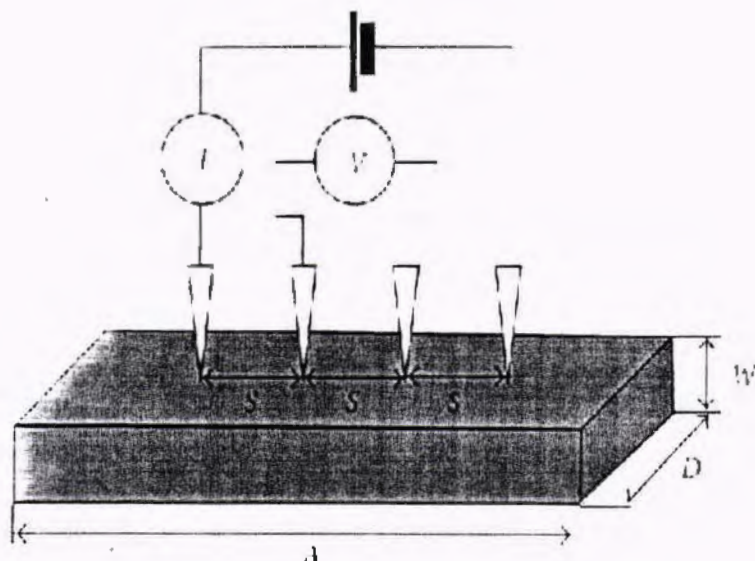


Fig 3.6: Diagram of four point probe setting.

Current of high impedance is supplied to the probe 1 and 4. Inner two probes 2 and 3 measure potential difference using voltmeter. Finally resistivity is determined. The spacing ($s=1\text{mm}$) is adjusted between the probes [62 63].

The current doesn't draw through inner probes because input impedance is high in the circuit. By measuring the potential difference, unwanted potential drop between contacts 2 and 3 and sample is eliminated. Resistivity is given by.

$$\rho = \frac{V}{I} 2\pi s \quad (3.4)$$

3.4.1 Measuring resistance of MTJ by Four point Probe method:

Four point probe is an effective method for the characterization of MTJs current in plane properties and different properties e.g. TMR and low RA etc.

As shown in the fig (3.7) four probes are placed over the junction. Outer probes are used for current and inner probes measure potential drop for the measurement of the resistance of junction [64]

structure has been successfully deposited. The further zooming of the film reveals the desired nanostructure more clearly in fig (c) we can see the smooth thin film structure as it was glued to the substrate. The surface looks wavy or as in an interwoven textile. As the thin films were grown over the AAO templates so we expect that the films were grown over the 1-D nano structures. We located two tiny spots where the deposition did not went as required, revealing the underneath structure of thin film which are NWs that can be seen in fig 4.9 (b) and (d). By the above data it can be considered that we can grow the NWs by decreasing the time of deposition.

4.8 EDS results of CoFeB thin film

The EDS measurements for CoFeB thin film deposited on Al substrate are given in fig. 4.10.

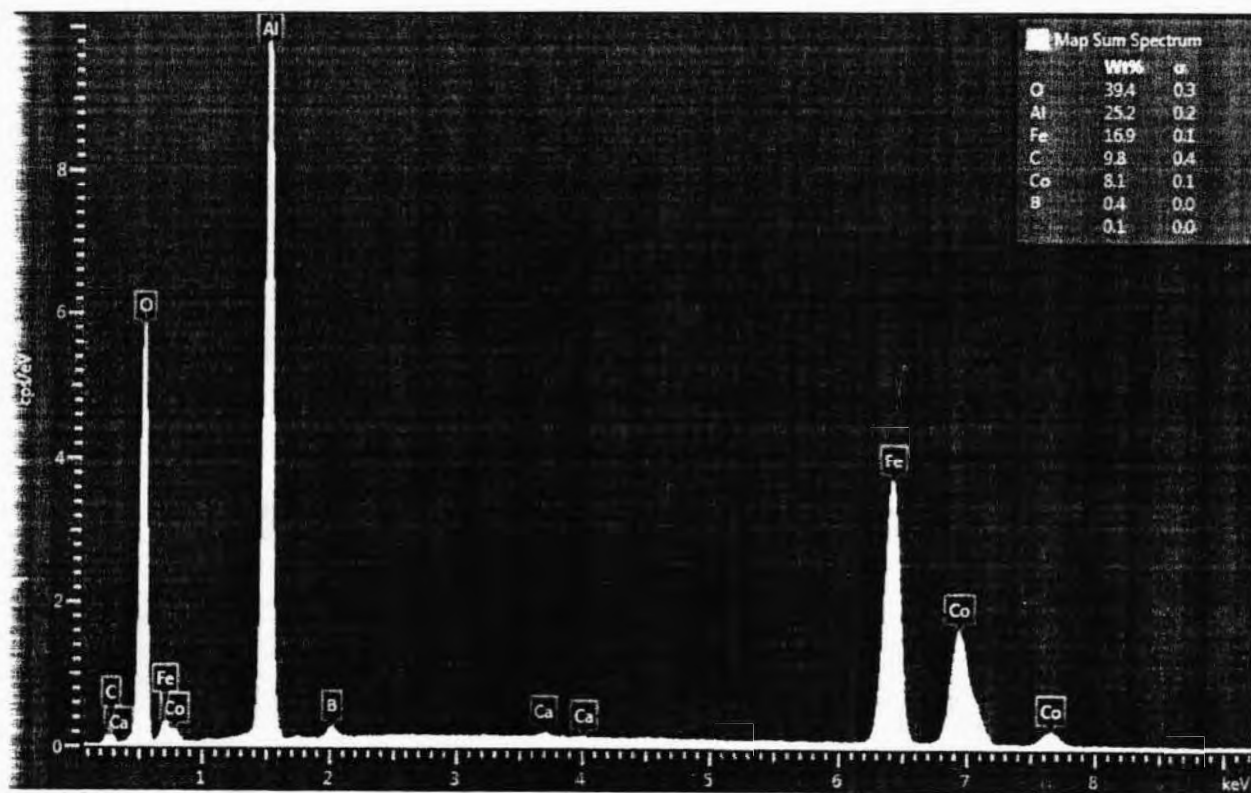


Fig. 4.10 EDS results of CoFeB thin film

It is confirmed by the EDS analysis that our required material has been deposited successfully. It can be seen that Fe and Co peaks are quite strong with a small peak of B because it is a lighter

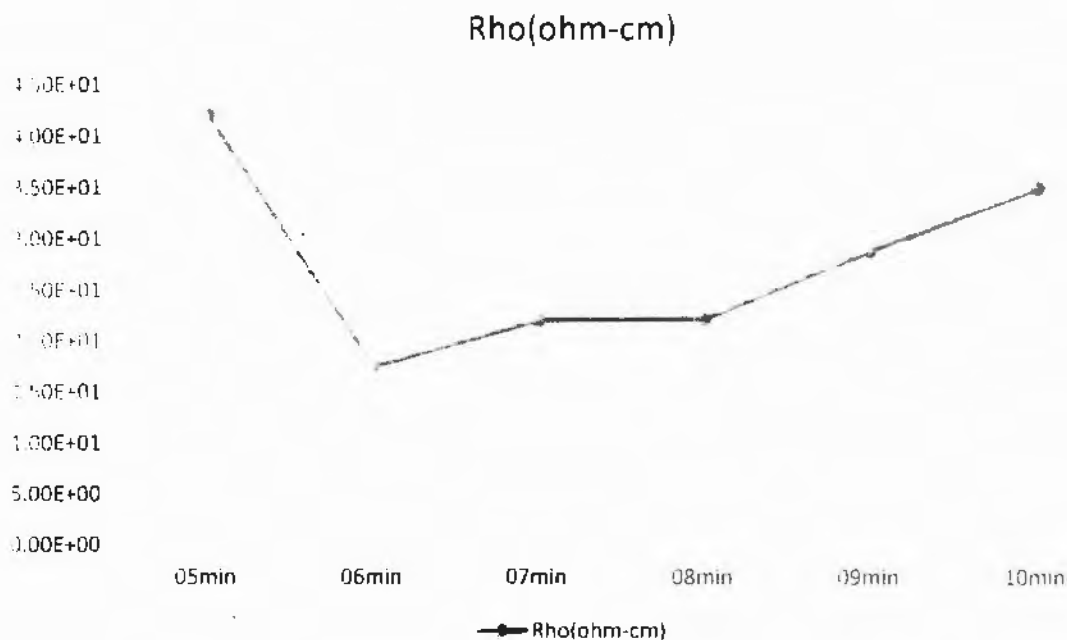


Fig 4.12 Graph for resistivity response with deposition time

The graph of resistivity shows that for sample prepared for 5 min deposition time we have max resistivity which decreases for higher deposition time and has gradual increase at the end but still not comparable to the sample 1. Which shows that the optimized conditions to gain max resistivity is as for sample 1. We conclude that for a specific thickness of film the resistivity is maximum.

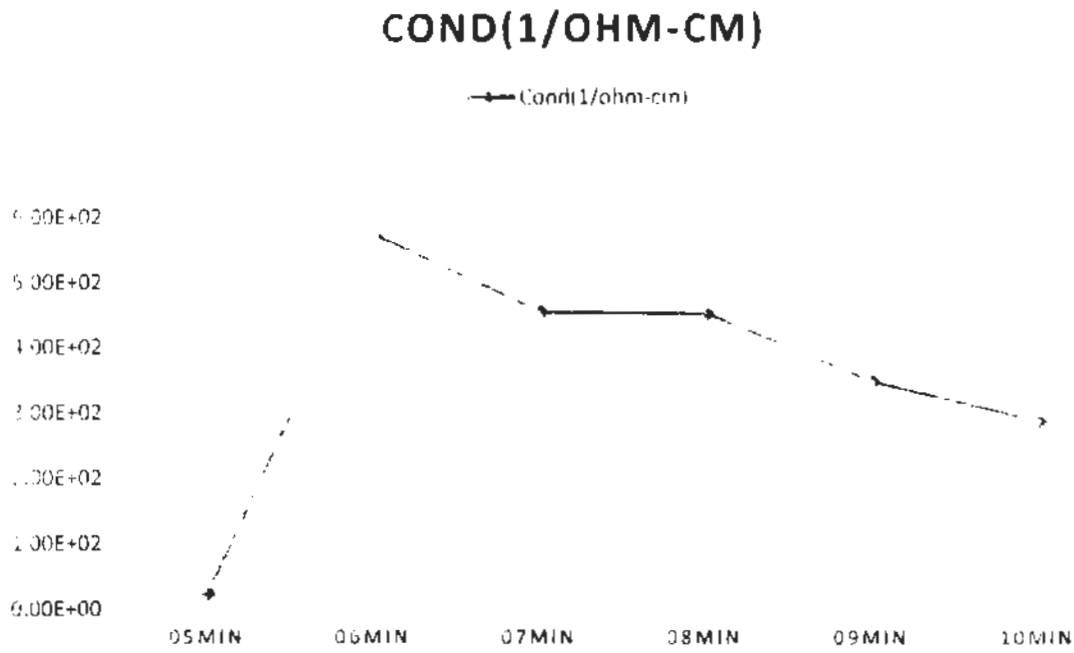


Fig.4.13 Graph for conductivity response with deposition time

The above graph is for conductivity for samples having different thickness. It can be seen that for sample 1 we have min conductivity which increases for sample 2 and then gradually decreases. This graph confirms the result from the graph of resistivity as we have min conductivity when the resistivity is maximum this again proves the conditions for sample 1 are the best to prepare the thin film.

3.4. Four point probe method:

Tungsten metal tips with spring supports having finite radius are used in this technique. They are spaced equally as shown in the fig (3.6). Springs prevent any damage to the sample by not pressing too hard on it and they can move up and down according to surface while characterization.

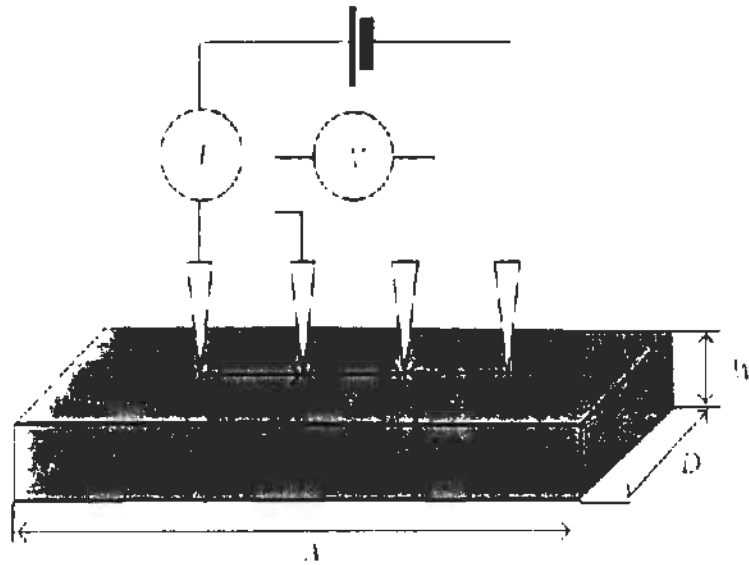


Fig 3.6: Diagram of four point probe setting.

Current of high impedance is supplied to the probe 1 and 4. Inner two probes 2 and 3 measure potential difference using voltmeter. Finally resistivity is determined. The spacing ($s=1\text{mm}$) is adjusted between the probes [62 63].

The current doesn't draw through inner probes because input impedance is high in the circuit. By measuring the potential difference, unwanted potential drop between contacts 2 and 3 and sample is eliminated. Resistivity is given by.

$$\rho = \frac{V}{I} 2\pi s \quad (3.4)$$

3.4.1. Measuring resistance of MTJ by Four point Probe method:

Four point probe is an effective method for the characterization of MTJs current in plane properties and different properties e.g. TMR and low RA etc.

As shown in the fig (3.7) four probes are placed over the junction. Outer probes are used for current and inner probes measure potential drop for the measurement of the resistance of junction [64]

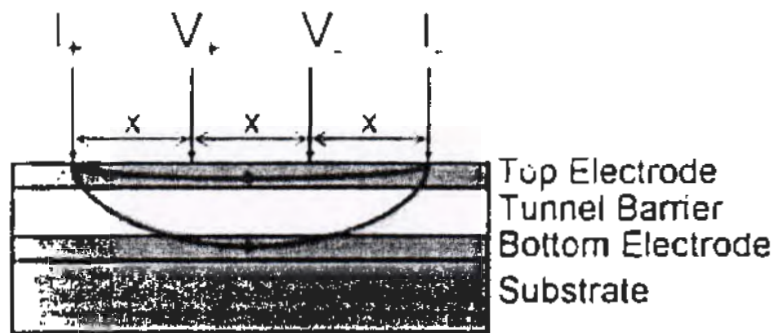


Fig 3.7: Schematic representation of current in plane tunneling method by four point probe.

Some part of current passes through the bottom electrode crossing the barrier. Probe spacing is important for the amount of flow of current through bottom electrode. All current flows through top electrode for small spacing and for large spacing between probes there will be proportion of current flow between top and bottom electrode. Distance between the probes is very important. By varying the probe distance the resistance of junction can be measured. For different barrier thickness the junction characteristics can be measured.

5 Vibrating Sample Magnetometer (VSM)

Vibrating Sample Magnetometer (VSM) is a device invented by Simon Foner in 1955 in Lincoln laboratory MIT [65]. It is a device widely used for the characterization of magnetic properties of a number of magnetic material types like paramagnetic, diamagnetic, ferromagnetic and anti-ferromagnetic materials. An electromagnet provides magnetizing field (DC) in VSM. A vibrator vibrates the sample sinusoidal in the presence of magnetic field, it is done with the help of piezoelectric material. Due to the change in flux that is generated by the vibrating sample the detection coils generates a signal voltage. The magnetic moment of sample can be measured by lock-in amplifier which is directly proportional to the induced voltage in pick up coils. Fig 3.8.

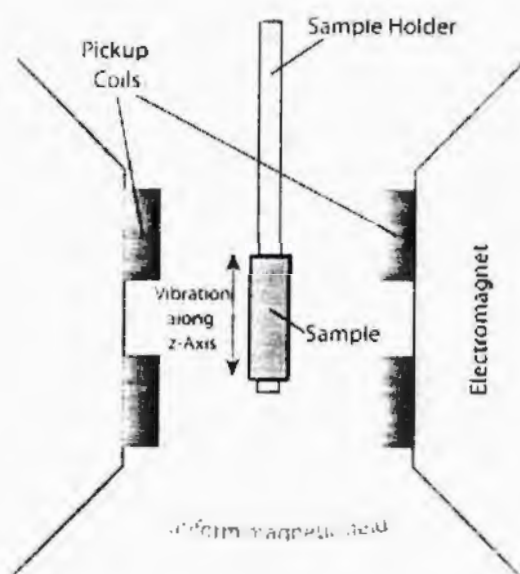


Fig.3.8: Structure of VSM.

Hysteresis curve of the material is obtained by this output which exhibits the magnetic moment M as a function of magnetic field H . VSM measures the magnetization by converting the dipole field of the sample into AC signals.

CHAPTER 4 Results and conclusion

4.1 Transport Properties of CoFeB/Al-O CoFeB:

Four probe technique is employed to calculate the TMR value of double barrier magnetic tunnel junction with SiO₂ and glass substrates. Readings were taken at room temperature and resistance of junction against applied magnetic field along the plane was measured.

4.2 TMR for the MTJ with glass substrate:

The figure 4.1 depicts the TMR values for the MTJ with glass substrate which was obtained 10%. The curve explains the switching of free electrode as well. The switching field depends on the coercivity of FM electrodes.

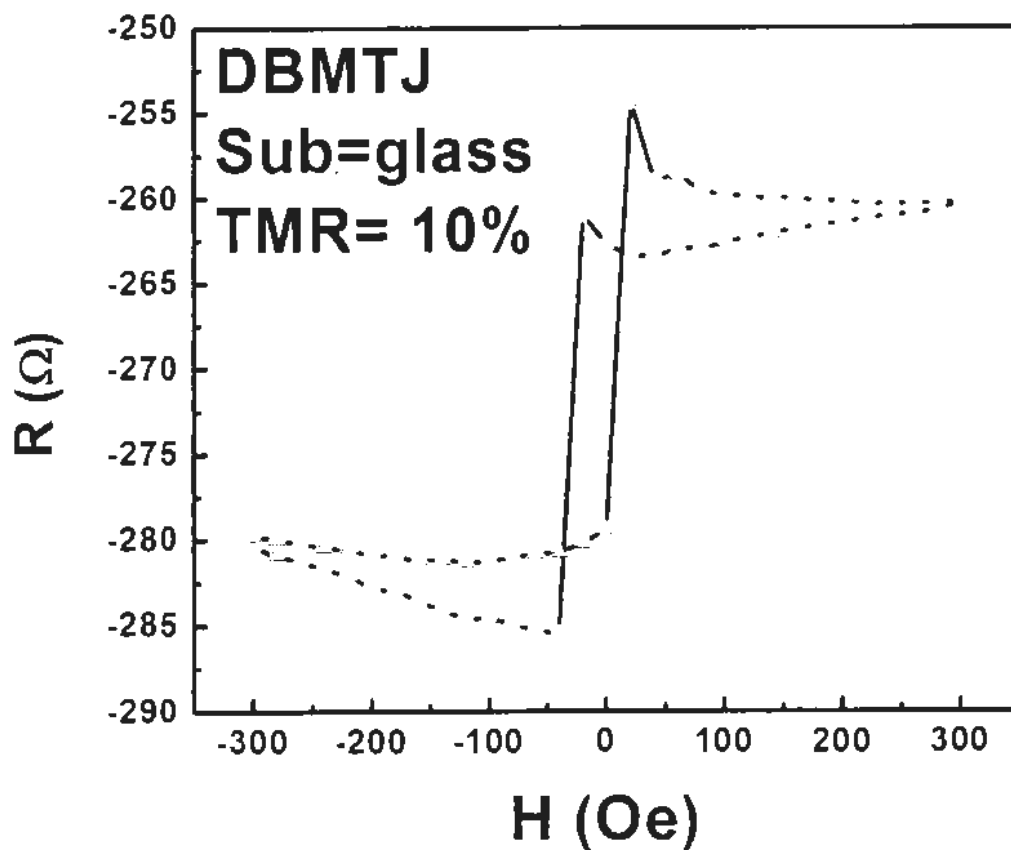


Fig: 4.1 Resistance Curve of DBMTJ at room temperature.

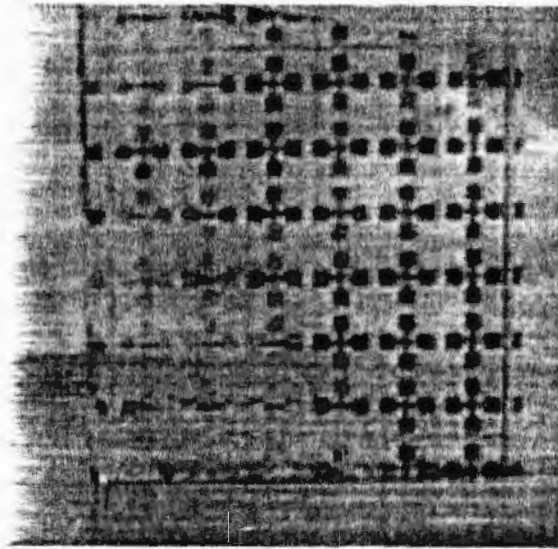
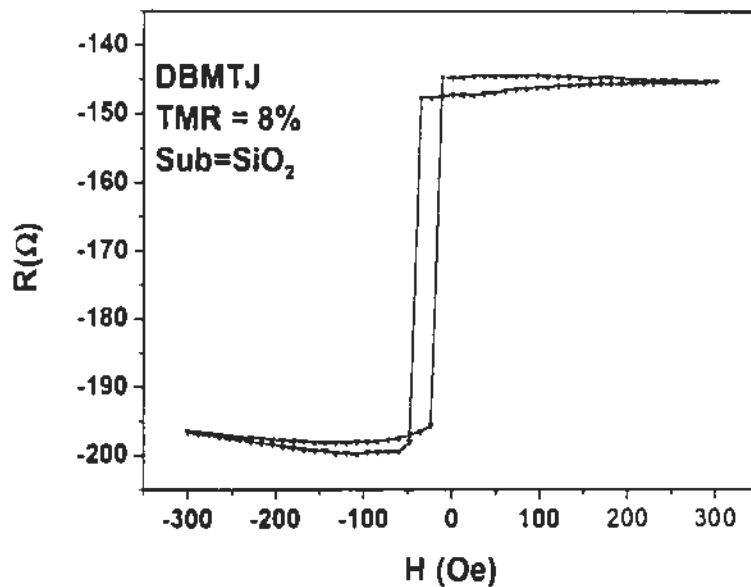
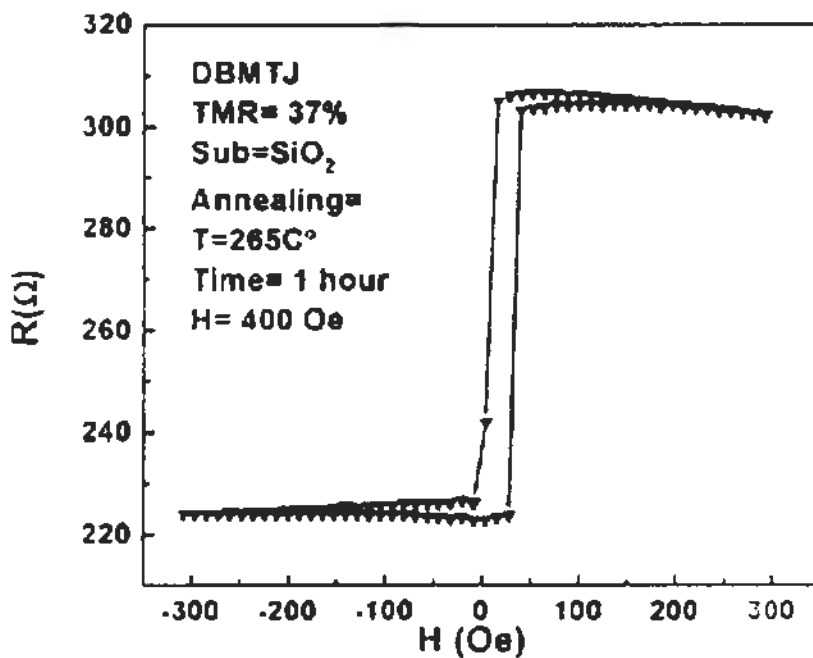


Fig. 4.2 Array of MTJs with glass substrate.

4.3 Effect of change of substrate in CoFeB/Al-O/CoFeB MTJ:

It is observed that by changing the substrate from glass to SiO₂ the TMR value of DBMTJ was decreased to 8%. The TMR with glass substrate is 10%. The sample with SiO₂ substrate was also annealed at 265°C for one hour in 400Oe field in the direction of easy axis. Which increased the TMR from 8% to 37%. It is concluded that the annealing of the MTJ with SiO₂ substrate has effect on the TMR values which has increased after annealing. The following factors are considered to be responsible for this change.

- (i) Improvement of ferromagnetic layer/barrier interface.
- (ii) Enhancement of the magneto crystalline anisotropy of magnetic layers
- (iii) Tunneling of mobile electrons
- (iv) Effect of substrate on the buffer layer

Fig 4.3 TMR curve for MTJ with SiO₂ substrate before annealingFig 4.4 TMR curve for MTJ with SiO₂ substrate after annealing

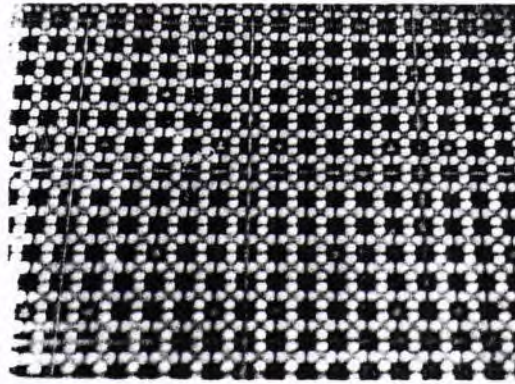


Fig. 4.5 Array of DBMTJs with SiO₂ substrate.

4.4 I-V Characteristic Curve for DBMTJ with glass substrate:

The MTJ provided for I-V characterization had CoFeB FM layers and AlO as insulating layer with 1 nm thickness sandwiched between the FM layers. The junction resistance was found to be from 40 to 100 Ω . I-V probing was done at different contact points. The graphs for different points are given below.

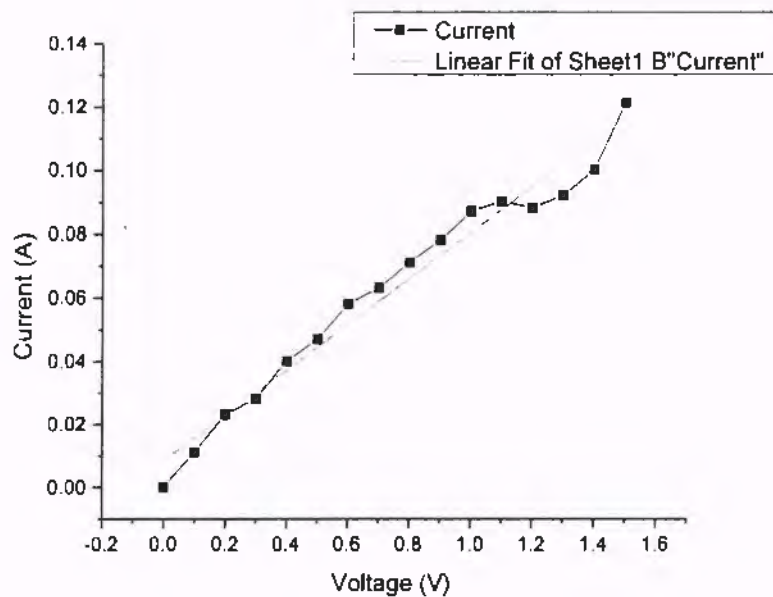


Fig. 4.6 I-V curve for Metallic-Metallic probing

The graph shows the behavior of I-V curve which is almost linear up to 1.1 V and the resistance is found 13 Ω .

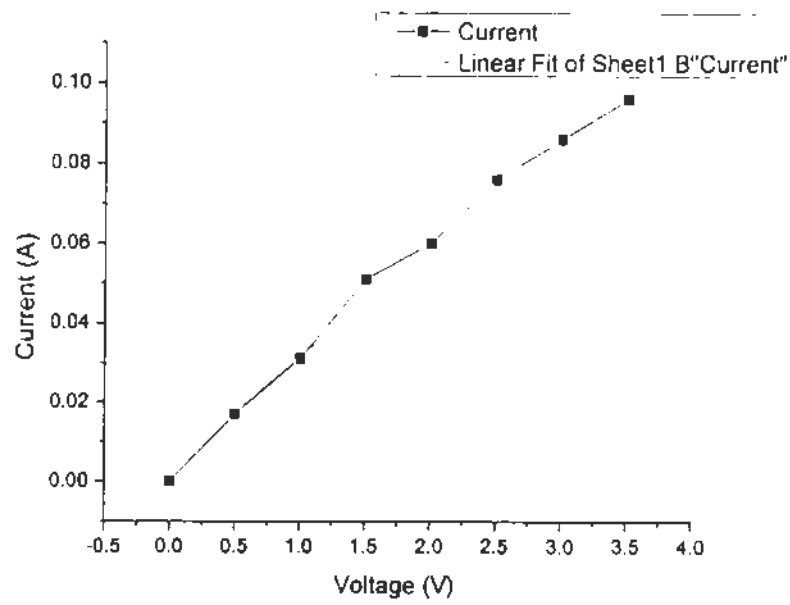


Fig. 4.7 I-V curve for Black-Black probing.

Resistance is $R=40 \Omega$.

4.5 I-V Characteristic Curve for DBMTJ with SiO₂ substrate:

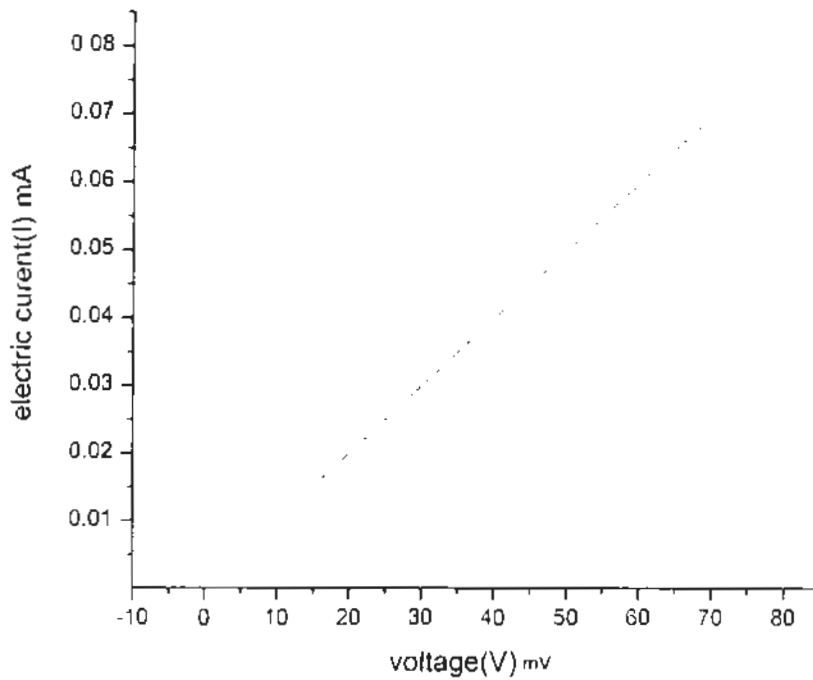


Fig. 4.8 Graph for I-V characteristic of DBMTJ with SiO₂ substrate.

The graph between applied voltage and current is linear for the double barrier magnetic tunnel junction deposited on SiO₂ substrate. Which is a different behavior compared to the I-V curve of DBMTJ with glass substrate. Which shows that the substrate also have effects on the I-V characteristics. The resistance of the junction is 100 Ω .

We have used the four point probe technique to measure the resistance of DBMTJ in anti-parallel state and obtained I-V curves which show nonlinear behavior in the device with glass substrate and linear behavior with the SiO₂ substrate which shows that the resistance is ohmic. It also justifies the tunneling process in DBMTJ.

4.5.1 Material Parameters for DBMTJ:

The following measurements are done from Nano-Chip Reliability grade Hall Effect System, with approx. 65nm thickness model for DBMTJ.

Table 4.1 Hall measurements of DBMTJ

Sample	Condition	R_s (ohm/sq)	Rho (ohm-cm)	Con (1/ohm-cm)	N_s (/cm ²)	N_s (/cm ³)	μ_s (cm ² /Vs)
DBMTJ	B=100G; I=1mA	3.16E+00	2.05E-05	4.87E+04	4.07E+16	6.26E+21	1.05E+02

The measurements confirm that the phenomenon of Hall Effect is occurring in the DBMTJ which could lead to the in-field switching of magnetic layers.

4.7 SEM images of CoFeB thin film

The SEM images of CoFeB thin film for different film areas are given in fig. 4.9.

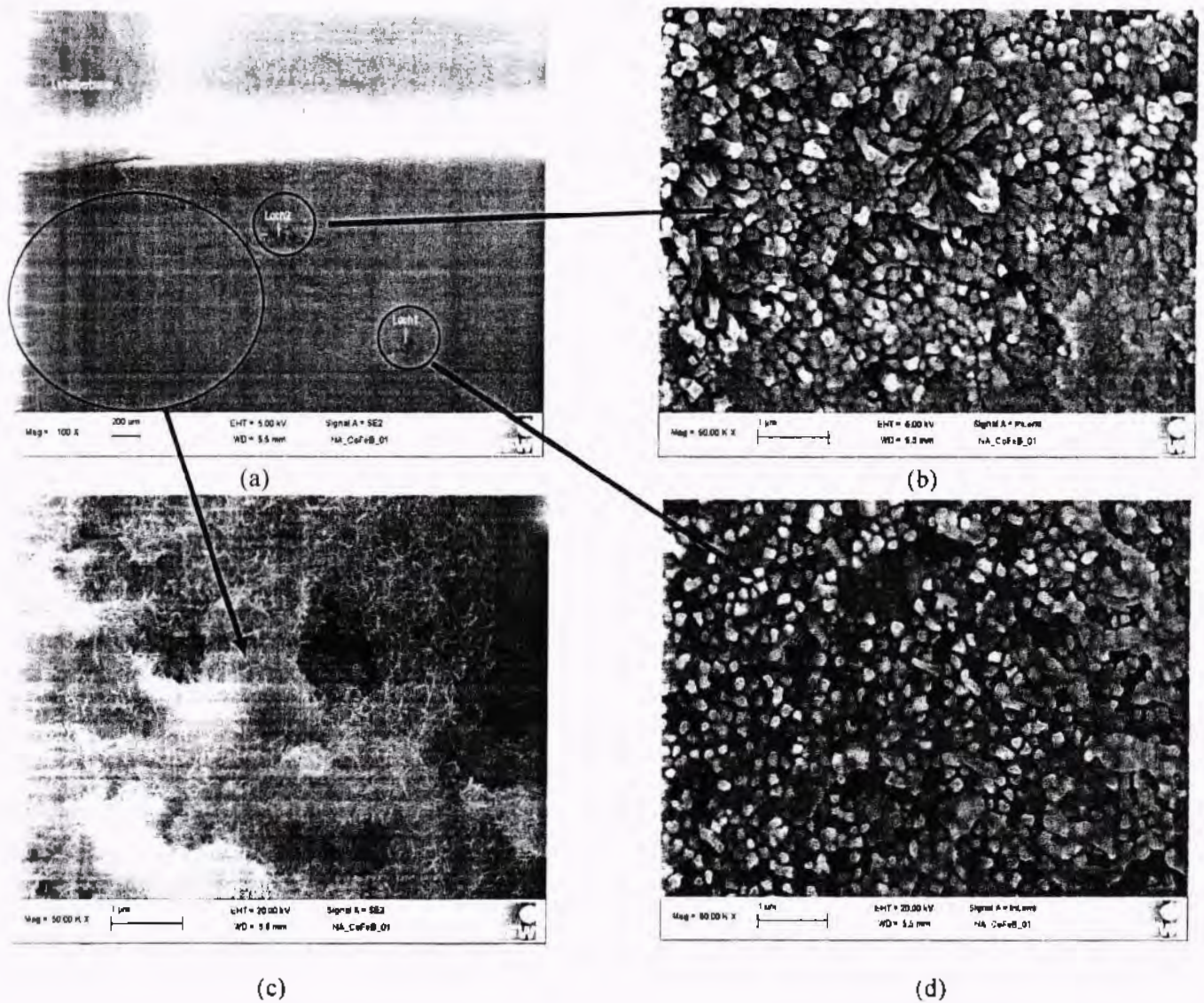


Fig 4.9 SEM images of CoFeB thin film

Thin films of CoFeB were deposited by electrodeposition method for different time periods. The SEM image shown in fig 4.9 is of the sample prepared at 5 min deposition time which was the minimum among the prepared samples. It can be clearly seen in fig. (a), that our desired thin film

structure has been successfully deposited. The further zooming of the film reveals the desired nanostructure more clearly in fig (c) we can see the smooth thin film structure as it was glued to the substrate. The surface looks wavy or as in an interwoven textile. As the thin films were grown over the AAO templates so we expect that the films were grown over the 1-D nano structures. We located two tiny spots where the deposition did not went as required, revealing the underneath structure of thin film which are NWs that can be seen in fig 4.9 (b) and (d). By the above data it can be considered that we can grow the NWs by decreasing the time of deposition.

4.8 EDS results of CoFeB thin film

The EDS measurements for CoFeB thin film deposited on Al substrate are given in fig. 4.10.

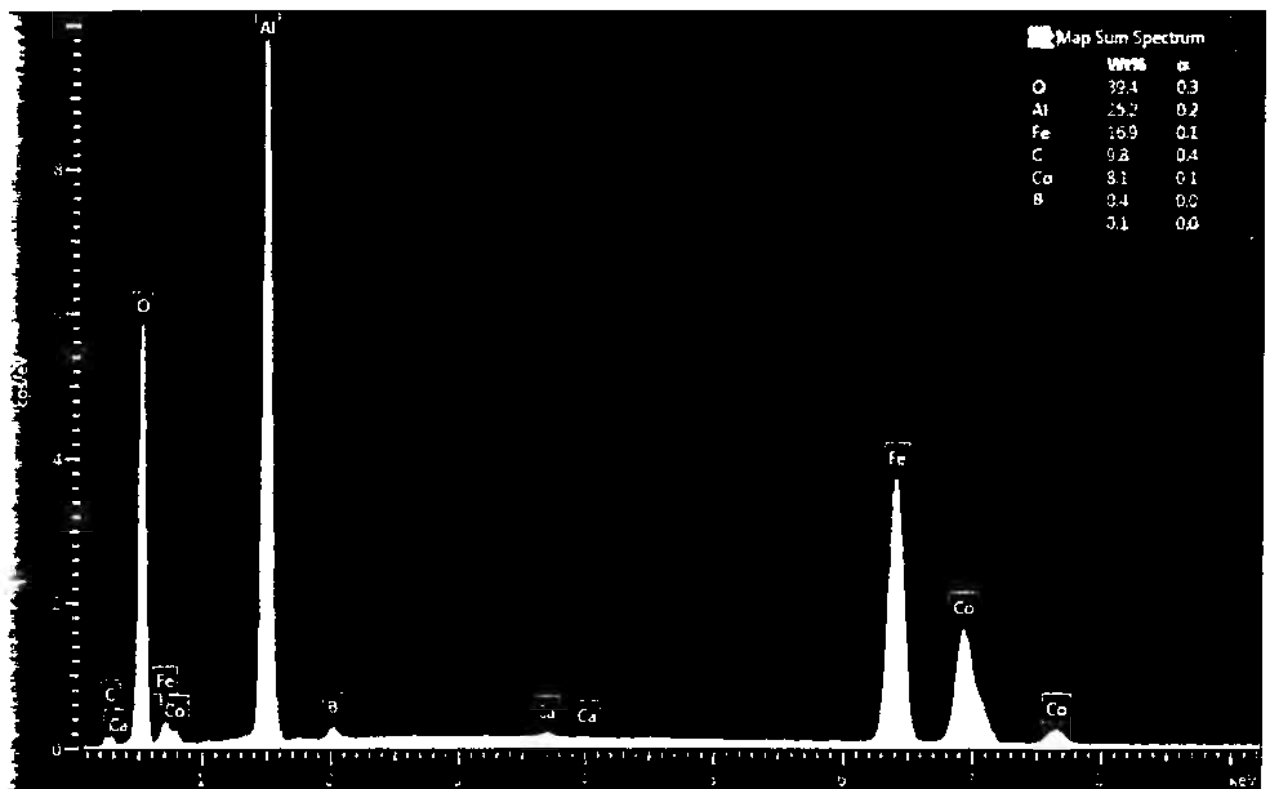


Fig. 4.10 EDS results of CoFeB thin film

It is confirmed by the EDS analysis that our required material has been deposited successfully. It can be seen that Fe and Co peaks are quite strong with a small peak of B because it is a lighter

element and difficult to detect. The Al peak is due to the aluminum substrate. The EDS results confirms the deposition of CoFeB which is the required thin film.

4.9 I-V characteristics of CoFeB thin film

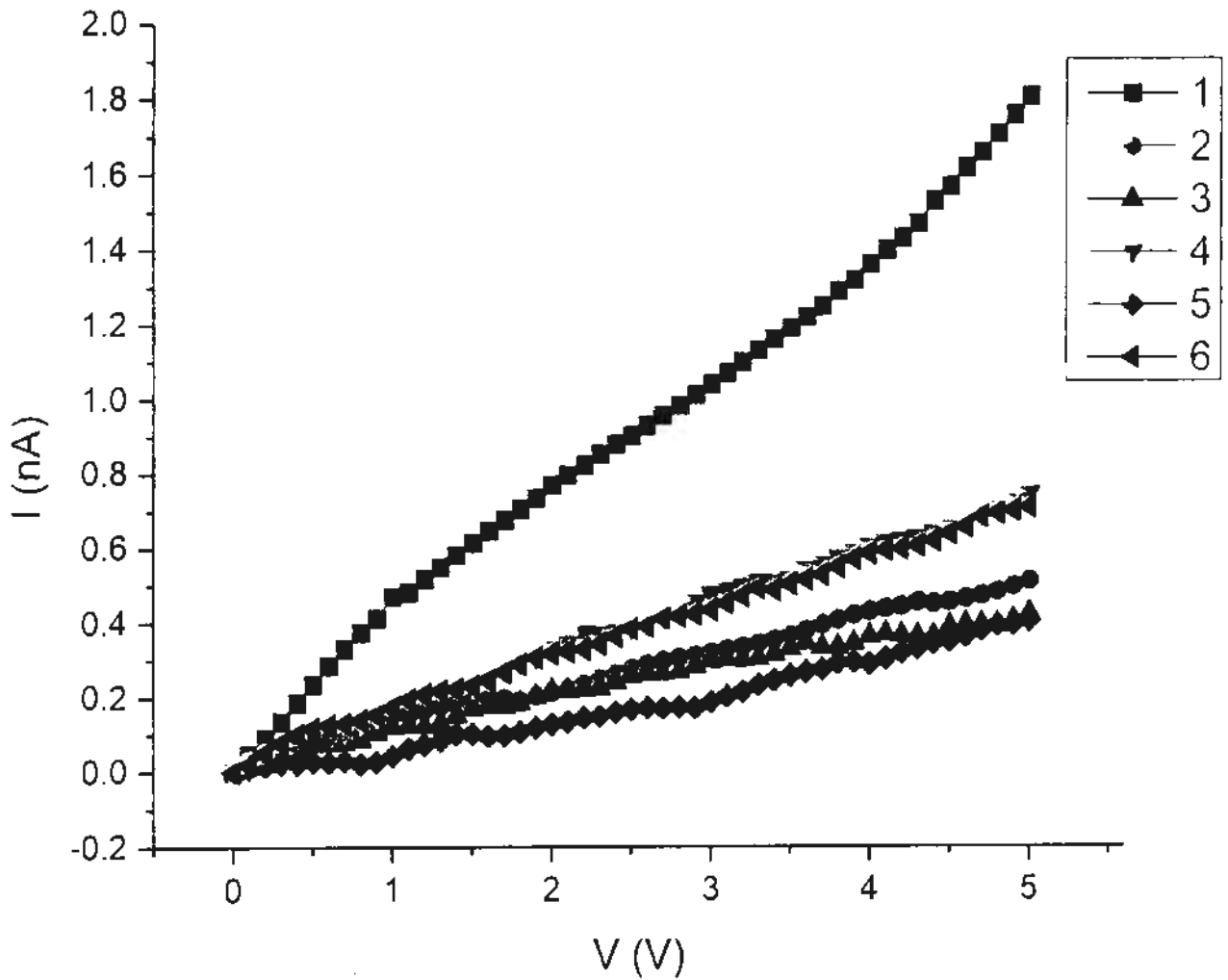


Fig. 4.11 I-V graph for CoFeB thin film with varying thickness.

The above graph shows the I-V data for the 6 samples of CoFeB thin film with varying thickness. The thickness of the samples was increased by increasing the time of deposition. The data of deposition is given in table 2.2. Sample 1 is deposited by giving the deposition time for 5 minutes. All other samples were prepared by a time gap of 1 minute each. The I-V graph shows that for

sample 1 the current increases almost linearly with increase in Voltage with a slight inclination between 4 and 5 volts. The I-V curves for other 5 samples having more thickness than the sample 1 responded differently as compared to the sample 1 and gave uncertain fluctuations between voltage and current. The graph shows that the current does not respond to the voltage for samples other than 1 as it does with the sample 1. The possible reason for this uncertain behavior could be the resistance response by increasing the thickness. The resistance fluctuates between 3-17ohms with variation in thickness. The curves which shows large amount of current upon the smaller value of voltages is because of larger concentration of iron as compared to boron and cobalt. We can also say that at this situation the charge density is larger due to which there is a trend of gradual increase in current in different samples of the compound and the corresponding curves as shown in the above graph.

4.10 Hall measurements for DBMTJ and CoFeB thin film:

The following measurements are done from Nano-Chip Reliability grade Hall Effect System, with assumed thickness of 70nm model for CoFeB thin film. We have taken the hall measurements both with the applied magnetic field and without the magnetic field. We have found that the Hall Effect occurs in the CoFeB thin film without any external applied field. This leads to the main phenomenon of spin Hall Effect for which no field is required for the spin accumulation on the lateral boundaries.

4.10.1 Hall measurements for CoFeB thin film:

Table 4.2. Hall measurements for the confirmation of spin Hall Effect.

Sample	Condition	Rs (ohm/sq)	Rho (ohm- cm)	Con (1/ohm- cm)	VH (V)	Ns (/cm ²)	Ns (/cm ³)	μs (cm ² /Vs)
CoFeB	With B	4.24E+05	2.97E-01	3.39E+00	-1.27E- 04	- 2.74E+11	- 3.92E+17	5.64E+01
CoFeB	Without B	3.57E+05	2.50E-01	4.09E+00	-1.94E- 04	- 2.95E+08	- 4.21E+14	6.50E+04

The above table (4.2) confirms the spin hall effect in the CoFeB thin film. The spin hall effect occurs without the applied external magnetic field. It can be seen that the Hall Effect occurs in thin film without the external magnetic field confirming the spin hall occurrence.

Table 4.3. Hall measurements for samples having different thickness by changing the deposition time.

Sample	Rs(ohm/sq)	Rho(ohm-cm)	Cond(1/ohm-cm)	N (/cm ³)	μ_s (cm ² /Vs)
1	6.01E+05	4.21E+01	2.38E+01	-7.88E+16	1.93E+01
2	2.08E+06	1.75E+01	5.72E+02	-7.47E+15	1.02E+02
3	2.30E+06	2.21E+01	4.53E+02	-8.74E+15	5.54E+01
4	1.98E+06	2.22E+01	4.51E+02	-1.22E+16	4.53E+01
5	2.29E+06	2.89E+01	3.46E+02	-4.35E+15	9.33E+01
6	2.50E+06	3.50E+01	2.86E+02	-7.19E+15	3.48E+01

Here, Rs: Sheet Resistance, B: Magnetic Field (G), Rho: Resistivity, Con: Conductivity, VH: Hall Voltage, Ns: Carrier Concentration, μ_s : Sheet Carrier Mobility.

The above table shows hall measurements taken for samples having different thickness. The table shows that sheet resistance and resistivity has more value in sample 1 as compared to the other samples and has less conductivity. Which makes it a good specimen for the obtaining the high TMR values. By analyzing the Hall measurements it can be said that the optimized condition for sample preparation are as for sample 1.

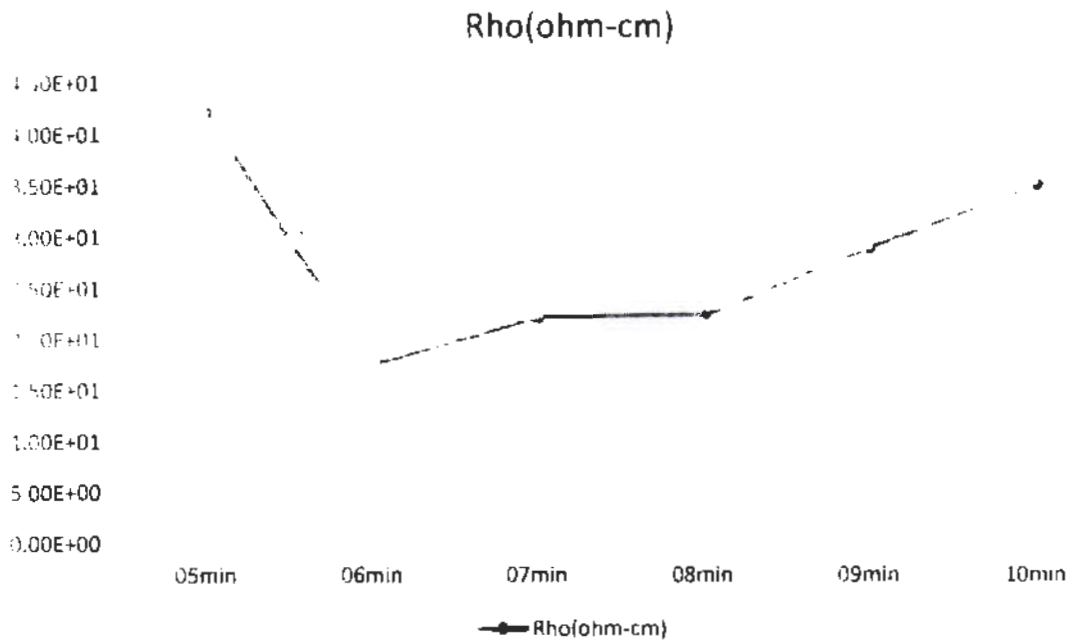


Fig 4.12 Graph for resistivity response with deposition time

The graph of resistivity shows that for sample prepared for 5 min deposition time we have max resistivity which decreases for higher deposition time and has gradual increase at the end but still not comparable to the sample 1. Which shows that the optimized conditions to gain max resistivity is as for sample 1. We conclude that for a specific thickness of film the resistivity is maximum.

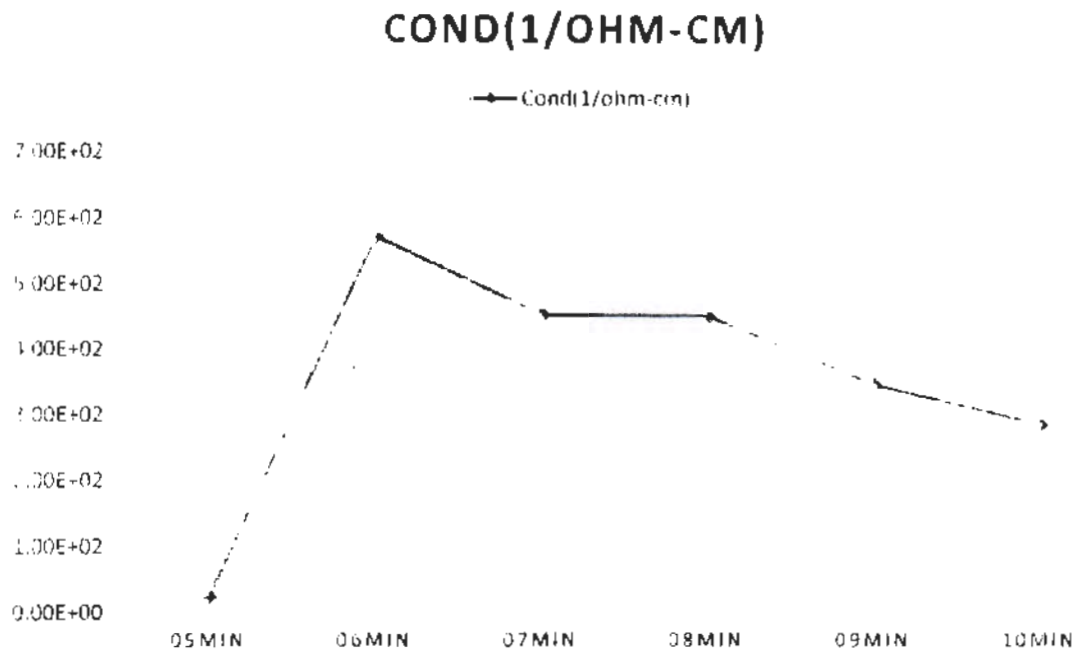


Fig.4.13 Graph for conductivity response with deposition time

The above graph is for conductivity for samples having different thickness. It can be seen that for sample 1 we have min conductivity which increases for sample 2 and then gradually decreases. This graph confirms the result from the graph of resistivity as we have min conductivity when the resistivity is maximum this again proves the conditions for sample 1 are the best to prepare the thin film.

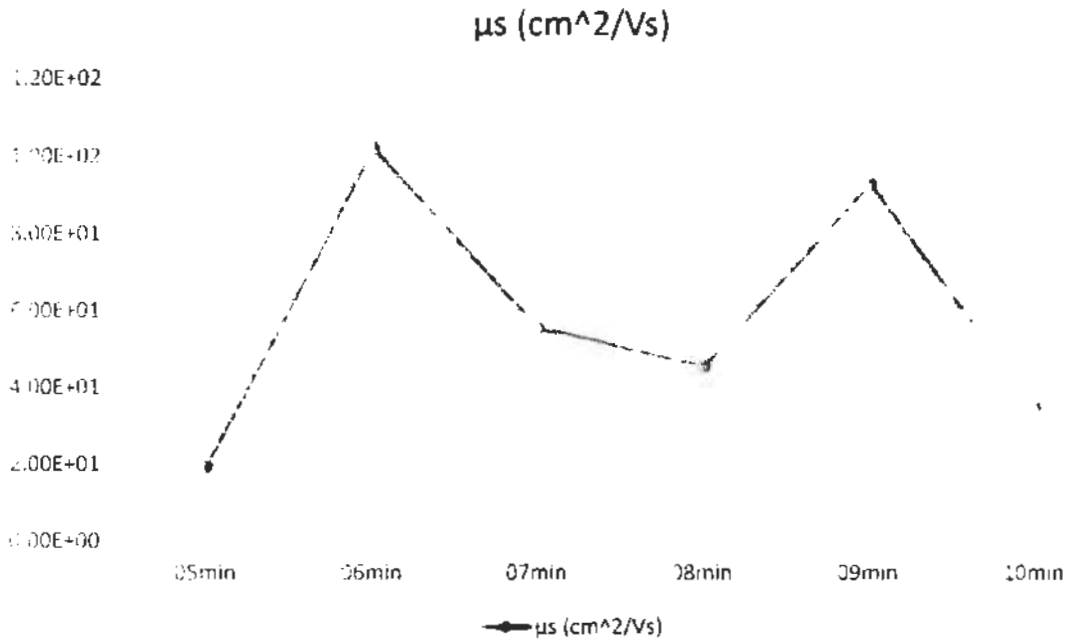


Fig 4.13 Graph for carrier mobility with deposition time

The charge carrier mobility graph has fluctuating values for different film thickness. The min value for mobility is for sample 1. This condition again confirms the above results of resistivity and conductivity as the mobility is lower when the resistivity is max and conductivity is min.

We can conclude that the sample 1 has all the characteristics to achieve higher TMR values as it has max resistivity and low conductivity and carrier mobility.

4.11 M-H loops of CoFeB thin films

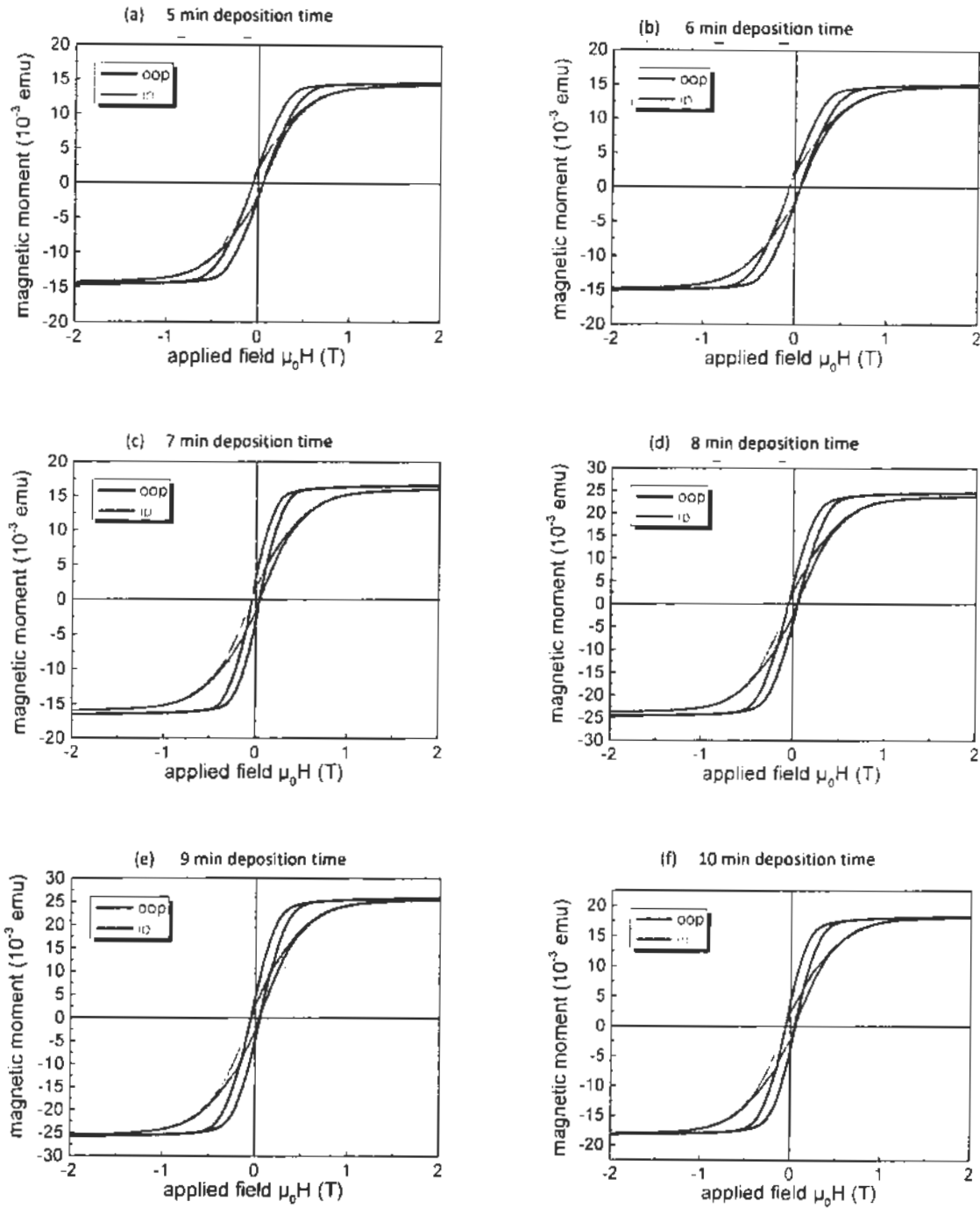


Fig 4.14 VSM measurements of CoFeB thin films.

The above graphs shows the VSM data acquired by characterizing the CoFeB thin films using (Quantum Design PPMS VSM) at various thickness. The thickness was varied by prolonging the deposition time. The obtained parameters form VSM are given below in the table 4.3.

Table 4.3 parameters obtained from VSM

sample	M_r (mT)	M_s (mT)	M_r/M_s	H_c (mT)
1	11.85	14.64	1.220E-1	59
2	11.62	14.92	1.284E-1	59
3	11.63	16.3	1.401E-1	45
4	10.85	24.1	2.715E-1	47
5	9.06	25.5	2.815E-1	49
6	10.15	18.1	2.988E-1	52

As we know that the squareness is M_r/M_s and here we characterize the sample along two angles. One is parallel and other is perpendicular external applied field (H) for each sample as shown in fig 4.14 (a-f). We correlate the squareness of each sample for which the thickness gradually increases (sample 1-6). By co relating we observed that the squareness along the perpendicular axis remains almost same and the squareness along parallel axis of the sample gradually decreases hence we conclude that the easy axis is out of plane for each sample. By comparing the 6 samples for squareness. We have found that for out of plane applied field the value of M_s and M_r has slight but constant increase with increasing the thickness. This effect is attributed to the Neel Wall motion.

Conclusion

Double barrier magnetic tunnel junction

Ru5/Cu20/Ru5/IrMn10/CoFe2.5/Ru0.8CoFeB3/Al1nmOx/CoFeB3/Al1nmOx/CoFeB4/Ru10Ta5/CoFe8/IrMn10/Ta3 was synthesized by the magnetron sputtering system, ion beam etching and photolithography on Glass substrate as well as on SiO₂ substrate at P=10⁻⁸Torr pressure. With the help of four point probe we have measured the Tunneling Magnetoresistance (TMR) and I-V curves at room temperature. The resistance of the junction is found to be from 40-100Ω from IV curve. The TMR value for DBMTJ with glass substrate is found to be 10% with 300Oe applied field in the plane of MTJ. After annealing at H=400Oe at T=265C for an hour and changing the substrate from glass to SiO₂ it is observed that TMR value has increased up to 37%. This increase in the TMR value is considered as a result of interface smoothing and crystallinity of FM layers, also the substrate may have effect on the buffer layer which led in the change of magnetization of junction. We have prepared CoFeB thin films by electrodeposition using AAO templates under varying conditions and taken different measurements. We have taken magnetic measurements which gave outstanding results. We concluded by squareness that the easy axis is out of plane for CoFeB thin film and the material showed ferromagnetic behavior. We have taken I-V curves and the hall measurements both with the applied magnetic field and without the magnetic field. We have found that the Hall Effect occurs in the CoFeB thin film without any external applied field. This leads to the main phenomenon of spin Hall Effect for which no field is required for the spin accumulation on the lateral boundaries. The confirmation of Hall Effect in the junction could lead a new approach in which spin Hall Effect can generate spin currents which are intense enough for the induction of spin transfer torque switching. It could be used for controlling the device that can be much better than the existing technologies. It is also concluded that the film thickness could have effect on the TMR values and has optimized values for max TMR.

References

- [1] Wolf S.A., Awschalom D.D, Buhrman R.A, Daughton J.M, von Molnar S, Roukes M.L, & A. Y. Chtchelkanova D.M, Spintronics: A spin-based Electronics vision for the future, *Science* **294**, 1488-1495 (2001).
- [2] Slonczewski J.C, Current-driven excitation of magnetic multilayers, *J. Magn. Mater.* **159**, L1 (1996).
- [3] Berger L, Emission of spin waves by a magnetic multilayer traversed by a current, *Phys. Rev. B* **54**, 9353 (1996).
- [4] Tsoi M, Jansen A.G.M, Bass J, Chiang W.C, Seck M, Tsoi V, & Wyder P, Excitation of a magnetic multilayer by an electric current, *Phys. Rev. Lett.* **80**, 4281-4284 (1998).
- [5] Tsoi M, Jansen A.G.M, Bass J, Chiang W.C, Tsoi V, & Wyder P, Generation and detection of phase-coherent current-driven magnons in magnetic multilayers, *Nature (London)* **406**, 46-48 (2000).
- [6] Katine J.A, Albert F.J, Ralph D.C, & Buhrman R.A, Current-induced realignment of magnetic domains in nanostructured Cu/Co multilayer pillars, *Appl. Phys. Lett.* **76**, 354 (2000).
- [7] Fuchs G.D, Emley N.C, Krivorotov I.N, Braganca P.M, Ryan E.M, Kiselev S.I, Sankey J.C, Katine J.A, Ralph D.C, & Buhrman R.A, Spin-transfer effects in nanoscale magnetic tunnel junctions, *Appl. Phys. Lett.* **85**, 1205 (2004).
- [8] Huai Y, Albert F, Nguyen P, Pakala M, & Valet T, Observation of spin-transfer switching in deep submicron-sized and low-resistance magnetic tunnel junctions, *Appl. Phys. Lett.* **84**, 3118 (2004).
- [9] Grollier J, Lacour D, Cros V, Hamzic A, Vaures A, Adam D, Faini G & Fert A, Switching the magnetic conformation of a spin valve by current induced domain wall motion, *J. Appl. Phys.* **92**, 4825 (2002).
- [10] Tsoi M, Fontana R.E & Parkin S.S.P, Magnetic domain wall motion triggered by an electric current, *Appl. Phys. Lett.* **83**, 2617 (2003).
- [11] Chiba D, Sato Y, Kita T, Matsukura F, & Ohno H, Current-driven magnetization reversal in a ferromagnetic semiconductor (Ga,Mn)As/GaAs/(Ga,Mn)As tunnel junction, *Phys. Rev. Lett.* **93**, 216602 (2004).

- [12] Elsen M, Bouille O, George J.M, Jaouors H, Mattana R, Cros V, Fert A, Lemaitre A, Giraud R, & Faini G. Spin transfer experiments on (Ga,Mn)As/(In,Ga) As/(Ga,Mn)As tunnel junctions, *Phys. Rev. B* **73**, 035303 (2006).
- [13] Engel B.N, Kerman J, Butcher B, Dave R.W, DeHerrera M, Durlam M, Grynkewich G, Janesky J, Pietambaram S.V, Rizzo N.D, Slaughter J.M, Smith K, Sun J.J & Tehrani S, A 4-mb toggle MRAM based on a novel bit and switching method, *IEEE Trans. Magn.* **41**, 132 (2005).
- [14] Gogl D, Arndt C, Barwin J.C, Bette A, DeBrosse J, Gow E, and Stefan Lammers H.H, Lamorey M, Lu Y, Mañtt T, Maloney K, Obermaier W. Sturm A, Viehmann H, Willmott D, Wood M. Gallagher W.J, Mueller G & Sitaram A.R, A 16-mb MRAM featuring bootstrapped write drivers, *IEEE J. Solid-State Circuits* **40**, 902 (2005).
- [15] Stockholm, Sweden, *Nano Letters* **8**(3), **805** (2008)
- [16] J Barnas J. *Phys.: Condense. Matter* **20**, 423202 (2008)
- [17] PY Clement *Appl. Phys. Lett.* **100**, 262404 (2012)
- [18] Yan Liuc, Yang Rena, Fulin Weia, P.P. Freitasb, *Applied Surface Science.* **314**, (2014) 443–446
- [19] R. Meservey, P.M. Tedrow, P. Fulde, *Phys. Rev. Lett.* **25**, 1270 (1970).
- [20] P.M. Tedrow, R. Meservey, *Phys. Rev. Lett.* **26**, 192 (1971).
- [21] R. Meservey, P.M. Tedrow, *Phys. Rep.* **238**, 173 (1994).
- [22] Valet and Fert, *Phys. Rev. B* **48**, 7099 (1993)
- [23] J.S. Moodera et al., *Phys. Rev. B* **42**, 8235 (1988)
- [24] Tedrow and Meservey, *Phys. Rev. Lett.* **27**, 919 (1971)
- [25] Baibich et al., *Phys. Rev. Lett.* **61**, 2472 (1988)
- [26] A. J. Annunziata, P. L. Trouilloud, S. Bandiera, S. L. Brown, E. Gapihan, E. J. O'Sullivan, and D. C. Worledge, *Journal of Applied Physics.* **117**, 17B739 (2015)
- [27] Seungkyo Lee, Kwangseok Kim, Injun Hwang, B.K. Cho *Current Applied Physics* **15**, (2015) 38–4
- [28] J. Y. Chen, N. Carroll, J. F. Feng, and J. M. D. Coey. *Appl. Phys. Lett.* **101**, 262402 (2012)
- [29] Léa Cuchet, Bernard Rodmacq, *Appl. Phys. Lett.* **103**, 052402 (2013)
- [30] K. Konishi, D. K. Dixit *Appl. Phys. Lett.* **102**, 162409 (2013)

- [31] Wolf S.A., Awschalom D.D., Buhrman R.A., Daughton J.M., von Molnar S., Roukes M.L., & A. Y. Chtchelkanova D.M., Spintronics: A spin-based electronics vision for the future, *Science* **294**, 1488–1495 (2001).
- [32] Valet T. & Fert A., Theory of perpendicular magnetoresistance in magnetic multilayers, *Phys. Rev. B* **48**, 7079 (1993).
- [33] Baibich M.N, Bronto J.M, Fert A, Dau F.N.V, Petroff F, Eitenne P, Creuzet G, Frederich A, & Chazelas J, Giant magnetoresistance in (001)Fe/(001)Cr magnetic superlattices, *Phys. Rev. Lett.* **61**, 2472 (1988).
- [34] Y. Sakuraba, M. Hattori, M. Oogane, Y. Ando, H. Kato, A. Sakuma, T. Miyazaki, and H. Kubota, Giant tunneling magnetoresistance in Co₂MnSi/Al–O/Co₂MnSi magnetic tunnel junctions. *Applied Physics Letters* **88** (2006) 192508.
- [35] M. Bowen, M. Bibes, A. Barthelemy, J.P. Contour, A. Anane, Y. Lemaitre, and A. Fert. Nearly total spin polarization in La_{2/3}Sr_{1/3}MnO₃ from tunneling experiments. *Applied Physics Letters* **82** (2003) 233.
- [36] W.H. Butler, X.G. Zhang, T.C. Schulthess, and J.M. MacLaren, Spin-dependent tunneling conductance of Fe|MgO|Fe sandwiches. *Physical Review B* **63** (2001) 054416.
- [37] Valet T. & Fert A., Theory of perpendicular magnetoresistance in magnetic multilayers, *Phys. Rev. B* **48**, 7079 (1993).
- [38] Baibich M.N., Bronto J.M., Fert A., Dau F.N.V., Petroff F., Eitenne P., Creuzet G., Frederich A., & Chazelas J., Giant magnetoresistance in (001)Fe/(001)Cr magnetic superlattices, *Phys. Rev. Lett.* **61**, 2472 (1988).
- [39] K. Matsuda, A. Kamijo, T. Mitsuzuka, and H. Tsuge, Exchange-biased magnetic tunnel junctions fabricated with in situ natural oxidation. *Journal of Applied Physics* **85** (1999) 5261.
- [40] L. Berger, “Emission of spin waves by a magnetic multilayer traversed by a current”. *Phys. Rev. B*, **54**, 9353, 1996.
- [41] J. C. Slonczewski, “Current-driven excitation of magnetic multilayers,” *Journal of Magnetism and Magnetic Materials*, vol. 159, 1-2, pp. L1-L7.S. S. P. Parkin, M. Hayashi, and L. Thomas, “Magnetic domain-wall racetrack memory.” *Science*, vol. **320**, no. 5873, pp. 190-4, Apr. 2008.
- [42] S. Dent, “Everspin throws first ST-MRAM chips down, launches commercial spintorque memory era,” *Engadget*, Nov. **14**, 2012,
- [43] J.E. Hirsch, “Spin Hall Effect,” *Phys. Rev. Lett.*, **83**, 1834–1837 (1999).

- [44] L. Liu, C.-F. Pai, Y. Li, H. W. Tseng, D. C. Ralph, R. A. Buhrman, "Spin-Torque Switching with the Giant Spin Hall Effect of Tantalum," *Science*, vol. **336**, pp. 555-558, 2012.
- [45] B. D. Cullity, C. D. Graham, *Introduction to Magnetic Materials*, Wiley-IEEE Press, United States, **94**, 2008.
- [46] M. Heide, G. Bihlmayer, and S. Blügel, "Dzyaloshinskii-Moriya interaction accounting for the orientation of magnetic domains in ultrathin films: Fe/W(110)," *Phy. Rev. B.*, 2008. **78**.
- [47] K.-S. Ryu, L. Thomas, S.-H. Yang, S. Parkin, "Chiral spin torque at magnetic domain walls." *Nature Nanotechnology*, vol. **8**, 2013.
- [48] S. Emori, U. Bauer, S.-M. Ahn, E. Martinez, G. S. D. Beach, "Current-driven dynamics of chiral ferromagnetic domain walls," *Nature Materials*, vol. **12**, 2013.
- [49] K.-S. Ryu, S.-H. Yang, L. Thomas, S. S. P. Parkin, "Chiral spin torque arising from proximity-induced magnetization," *Nature Communications*, **5**, 3910 (2014).
- [50] P. P. J. Haazen, E. Murè, J. H. Franken, R. Lavrijsen, H. J. M. Swagten, B. Koopmans. "Domain wall depinning governed by the spin Hall effect," *Nature Materials*, vol. **12**, April 2013.
- [51] M. A. Liberman, *IEEE Trans. Plasma Sci*, PS-17, 338 (1989).
- [52] D. Vender, R. Boswell, *J. Vac. Sci. Tech. A*10, 1331 (1992).
- [53] P. M. Vallinga, P. M. Meijer, F. J. de Hoog, *J. Phys. D. Apply. Phys.* **22**, 1650(1989).
- [54] G. R. Misium, A. J. Lichtenberg, M. Liberman, *J. Vac. Sci. Tech. A*7, 1007(1989).
- [55] "An automated system for measuring the complex impedance and its relaxation in softmagnetic materials", J.P. Sinnecker, M. Knobel, M.L. Sartorelli, J. Schonmaker, F.C.S. Silva, *J. de. Phys. IV Vol.8 No.2*. 665 (1 998).
- [56] "An introduction to physics and technology of thin films", A. Wagendristel, Y. Wang, World Scientific Publishing, pp3 1-40, (1 994).
- [57] K. Marutama, S. Endo, G. Sasaki, K. Kamata, J. Nishino, K. Kuchitsu, *J. Mat. Sci.Lett.*11, 1588 (1992).
- [58] H. S. Kwok, *Appl. Phys. Lett.* **59**, 3543 (1991).
- [59] S. Jasliree, R. Padiyali, 'I'. H. Rasmussen, S. V. Babu, *Appl. Phys. Lett.* **63**, 473(1993).
- [60] Foner, Simon (1 959). "Versatile and Sensitive Vibrating Sample Magnetometer". *Rev.Sci Instrum.* **30**, 548-557. doi: 10.1063/1.17 16679
- [61] M. T. Postek, K. S. Howard, A.H. Johnson and K. L. McMichael, Scanning electron microscopy Ladd Research Ind., Inc. Williston, **78**, (1980)

- [62] Smits FM. Measurement of sheet resistivities with the four-point probe. *Bell System Technical Journal*. **1058**, (2014)
- [63] Yi Lu and John R Bowler 2012 *Meas. Sci. Technol* **23** 1 15603. doi:10.1088/0957 023312311 111 15603
- [64] D.C. Worledge and P.L. Trouilloud, *Appl. Phys. Lett.* **83**, 84 (2003)
- [65] S. Ikeda, J. Hayakawa, M. L. Young, F. Matsukura, Y. Ohno, T. Hanyu, H. Ohno, *IEEE Trans. Electron Devices*. **54**, 991 (2007).
- [66] C. Chappert, A. Fert, F. N. V. Dau, *Nat. Mater.* **6**, 813 (2007).
- [67] J. C. Slonczewski, J. Z. Sun, "Theory of voltage-driven current and torque in magnetic tunnel junctions," *Journal of Magnetism and Magnetic Materials*, **310**, 169-175 (2007).
- [68] M. Hayashi, "Current Driven Dynamics of Magnetic Domain Walls in Permalloy Nanowires, Stanford University. **37**, (2006).
- [69] Faizan Ahmad, Dr Naeem Ahmad, "Spin dependent tunneling in spintronics nanostructures" Research thesis, (2015).

Turnitin Originality Report

DBMTJs and CoFeB by Fahad Hassan

From MS Thesis (MS Thesis)

Processed on 24-May-2016 16:59 PKT

ID: 677839599

Word Count: 11989

Similarity Index	Similarity by Source	
9%	Internet Sources:	2%
	Publications:	7%
	Student Papers:	3%

sources:

- 1 2% match (publications)
Handbook of Spintronics, 2016.
- 2 1% match (student papers from 10-Nov-2015)
Submitted to Higher Education Commission Pakistan on 2015-11-10
- 3 1% match (Internet from 22-May-2016)
<http://xxx.lanl.gov/pdf/cond-mat/0405528v1>
- 4 1% match (Internet from 28-Jan-2010)
<http://www.city.ac.uk/sems/dps/mathematics/mtj.pdf>
- 5 < 1% match (student papers from 11-Apr-2016)
Submitted to Nanyang Technological University, Singapore on 2016-04-11
- 6 < 1% match (publications)
"TMR and Al-O Based Magnetic Tunneling Junctions", Handbook of Spintronics, 2015.
- 7 < 1% match (publications)
Wen, Peifeng, "Spin polarized tunneling and spin injection in Fe-GaAs hybrid structures", Publikationsserver der Universität Regensburg, 2006.
- 8 < 1% match (publications)
- 9 < 1% match (Internet from 17-Nov-2014)
http://environnement.wallonie.be/rapports/owd/dechets_managers/ibh_cadet/ulg_renzoni.pdf